SABA Publishing

Journal of Mathematical Analysis and Modeling
jmam.sabapub.com
ISSN 2709-5924

J Math Anal & Model
(2025)6(2) : 60-99
doi:10.48185/jmam.v6i2.1681

Classical optimal single-step hybrid block techniques for ODEs: Combined basis functions with dynamic collocation strategy

O. V. ATABO[a,*], A. T. COLE[b], S. O. ADEE[c], P. O. OLATUNJI[d], E. O. OMOLE[e], Q. O. AHMAN[f]

[a,f] Department of Mathematics and Statistics, Confluence University of Science and Technology, Osara, Kogi State, Nigeria
[b] Department of Mathematics Federal University of Technology, Minna, Niger State, Nigeria
[c] Department of Mathematics, Modibbo Adama University, Yola, Adamawa State, Nigeria
[d] Department of Mathematical Sciences, Adekunle Ajasin University, Akungba-Akoko, Ondo, Ondo State, Nigeria
[e] Department of Physical Sciences, Mathematics Programme, Landmark University, Omu-Aran, Kwara State, Nigeria.

• *Received: 03 July 2025* • *Accepted: 12 September 2025* • *Published Online: 05 November 2025*

Abstract

We introduce a new class of block methods based on a hybrid basis of Hermite probabilists' polynomials and exponential polynomials. The proposed techniques exploit the complementary strengths of both families, offering enhanced accuracy, stability, and flexibility compared with schemes built on a single polynomial type. The methods employ interpolation and dynamic collocation and are formulated within a second-derivative framework. To strengthen their structure, additional terms are generated through the recurrence relation of Hermite probabilists' polynomials, whose orthogonality provides further advantages over exponential functions. Since the accuracy of numerical methods depends largely on discretization constants, this hybridization, together with the clustered mesh points, help reduce discretization errors and error constants while maintaining stability. Rigorous theoretical analysis establishes A-stability and convergence of the schemes. Although their algebraic order of convergence is relatively low, numerical experiments demonstrate that the methods achieve improved accuracy and competitive precision factors compared with existing block approaches. These results suggest that hybrid polynomial bases provide a promising pathway for the development of robust and efficient block algorithms in numerical analysis.

Keywords: Dynamic collocation approach, orthogonal polynomials, multi-derivatives, optimal methods.

1. Background of the study

In this study, we give attention to the formulation and implementation to calculating the near approximation solution to the true solution of ordinary differential equations (ODEs)

*Corresponding author: ataboov@custech.edu.ng

of the form

$$\phi'(x) = f(x, \phi(x)), \qquad \phi(x_0) = x_0, \qquad x \in [x_0, x_N], \qquad \phi, f \in \Re^d, \tag{1.1}$$

where d is the dimension of Equation (1.1) with the starting-value and initial solution as x_0 and ϕ_0, ϕ and f taken to satisfy Lipchitz's condition, existence and uniqueness theorems. Again, the choice of basis functions in numerical methods plays a critical role in determining the stability, accuracy, and efficiency of the resulting schemes, particularly when applied to different types of differential equations [1]. Ordinary differential equations (ODEs) arise in a wide range of applications, including control theory, engineering, physics, chemotaxis models, epidemiology, applied microbiology, and biotechnology [2]. Addressing the challenges posed by uncertain or fuzzy initial conditions, [3] developed an autonomous block two-step method and analyzed its zero-stability under fuzzy perturbations. To further enhance accuracy, [4] proposed a one-step, three-parameter optimized hybrid block method for first-order IVPs, while [5] and [6] introduced adaptive step-size hybrid block methods for both first- and second-order problems. Among these, one-step hybrid Obrechko-type block methods, derived through collocation at step and off-step points, have been shown to be consistent, zero-stable, and convergent, with numerical experiments confirming their superior accuracy and efficiency. Recent advancements even integrate machine learning techniques, such as feed-forward neural networks, into hybrid block methods to further improve numerical performance for first-order IVPs (see [7], [8]). The development of stable and efficient numerical schemes has been further advanced through the use of various polynomial basis functions. Methods based on Taylor series, power series, shifted Legendre polynomials, exponential functions, Laguerre polynomials, and Hermite probabilists' polynomials have been widely explored [9]. For instance, power series have been employed to construct linear and fourth-derivative block methods for third-order IVPs, achieving high-order accuracy and convergence (see [10], [11]), while Hermite polynomial-based approaches have enabled optimal-order approximations for first-order equations with confirmed stability and efficiency [12]. Building on these advances, hybrid block methods have incorporated dual-polynomial bases to reduce round-off errors (see [13], [14], [15]) and optimized half-step or second-derivative schemes to improve precision and robustness for stiff problems (see [16], [17]). These developments collectively demonstrate that carefully chosen polynomial bases can significantly enhance the performance of block methods across a variety of differential equation problems. Beyond theoretical improvements, block methods have been successfully applied to practical engineering and physical problems. Single-step and multi-derivative block schemes have been employed to simulate complex motion dynamics, integrate forced oscillatory systems, and solve higher-order ODEs with reduced computational cost (see [18], [19], [20], [21]). More recent contributions extend these techniques through continuous interpolation and collocation, allowing the simultaneous construction of main and complementary block schemes ([22]). Rigorous analyses of these approaches—including order of accuracy, error constants, stability, and convergence—combined with numerical experiments, confirm that block implementations enhance computational efficiency and reliability, often outperforming existing multi-derivative methods in both accuracy and robustness.

2. Motivation of the study

This study combines Hermite probabilists' and exponential polynomials to exploit their complementary strengths: Hermite polynomials are well suited for oscillatory problems, while exponential polynomials effectively approximate stiff problems. Based on these functions, we propose a class of single-step intra-step block methods constructed via dynamic collocation. The resulting schemes aim to deliver improved accuracy, stability, and flexibility. The methods are of a second-derivative type, with one variant incorporating an after-mesh or clustered mesh point. A major advantage is the reduced number of function evaluations in both derivation and implementation, which limits round-off errors, local truncation errors and accelerates convergence, since a few mesh points are taken. Efficiency is further enhanced by employing the Newton–Raphson approach at the implementation stage. The main limitation lies in the uncertainty of achieving strong stability properties through dynamic collocation, as continuous formulations are required to obtain $A-$, $L-$, $A(\alpha)-$, $\xi-$, or $p-$stable methods. The additional derivative in the formulas may also present practical challenges for implementation, as users may be reluctant to compute or program such derivatives for iterative procedures.
The paper is organized as follows: Section 1 presents the background, and Section 2 outlines the motivation. Section 3 develops the proposed methods, while Section 4 analyzes their numerical properties. Implementation procedures are discussed in Section 5, with applications and numerical results provided in Section 6. A detailed discussion follows, and Section 7 concludes with directions for future research.

3. The mathematical formulation

In this research, a combined polynomials basis functions, Hermite Probablist's and exponential polynomials functions below are used as approximate solution to Equation (1.1)

$$y(x) = \sum_{j=0}^{\nu} a_j H_j(x) + a_{\nu+u} \sum_{i=0}^{\nu+u} \frac{\alpha^i x^i}{i!}, \tag{3.1}$$

with the first and second derivatives given as

$$y'(x) = \sum_{j=0}^{\nu} a_j H_j'(x) + a_{\nu+u} \sum_{i=0}^{\nu+u} \frac{\alpha^i x^{i-1}}{(i-1)!}, \tag{3.2}$$

$$y''(x) = \sum_{j=0}^{\nu} a_j H_j''(x) + a_{\nu+u} \sum_{i=0}^{\nu+u} \frac{\alpha^i x^{i-2}}{(i-2)!}, \tag{3.3}$$

and the recursive formula for probailist's Hermite polynomials takes the form:

$$H_{j+1}(x) = xH_j(x) - H_j'(x), \qquad j = 0\ldots, \tag{3.4}$$

with $H_0(x)$ normalized, the first eight probabilist's Hermite polynomials are obtained from Equation (3.4) as:

$$\begin{aligned}
H_1(x) &= x,\\
H_2(x) &= x^2 - 1,\\
H_3(x) &= x^3 - 3x,\\
H_4(x) &= x^4 - 6x^2 + 3,\\
H_5(x) &= x^5 - 10x^3 + 15x,\\
H_6(x) &= x^6 - 15x^4 + 45x^2 - 15,\\
H_7(x) &= x^7 - 21x^5 + 105x^3 - 105x,\\
H_8(x) &= x^8 - 28x^6 + 210x^4 - 420x^2 + 105.
\end{aligned}$$

The polynomials plots for the Hermite probabilist's above are displayed to show the functional behaviour in the derivation of the intended optimal schemes in terms of numerical stability. You will quickly observe from Figure 1 that the zeros of the first six (6) of the probabilist's Hermite polynomials are smooth while the last two alternate, indicating that the former could produce acceptable numerical approximation by any derived numerical method if used as a basis function, since it provides good approximation to oscillatory-like differential systems. Consequently, this leads to reduced error constants and discretization errors. Besides, Hermite polynomials are orthogonal with respect to the weight function $w(x) = e^{-x^2}$ on the interval $(-\infty, \infty)$. where v and u are the number of polynomials

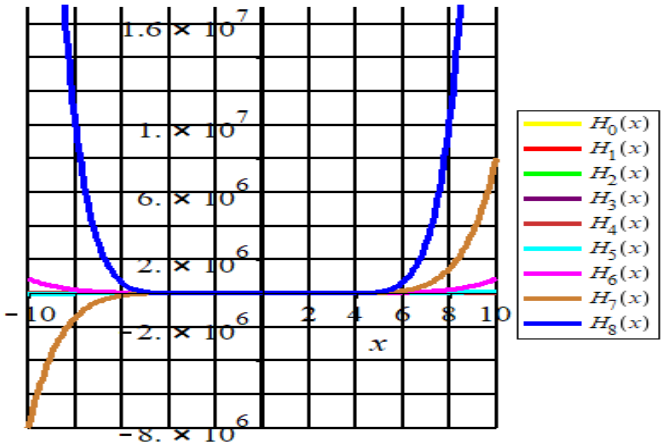

Figure 1: The probabilist's Hermite polynomials plots for $H_j(x), j = 0 \ldots 8$

respectively. For the specification of the suggested formulas, we take $v = 3$ and $u = 1$. However, the function $H_j{}'s$ and x are continuously differentiable, while the parameters $\alpha_j{}'s$ and α^i in Equations (3.1)–(3.3) are to be determined. Therefore, the block figures for the first and second proposed formulas are presented below. Now, interpolating Equation (3.1) at $x = x_n$ and collocating Equations (3.2) and (3.3) at $x = x_n, x_{n+1}, x_{n+\frac{3}{2}}$, while using Equation (3.4) gives an $n - by - m$ system of equations that can be put in

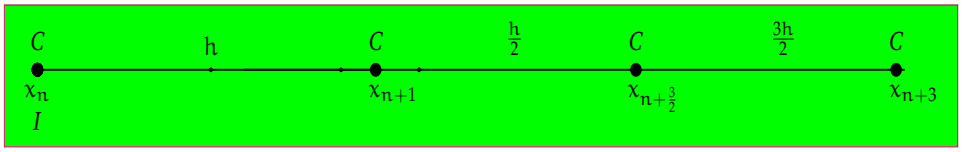

Figure 2: The classical optimal technique block figure COT1

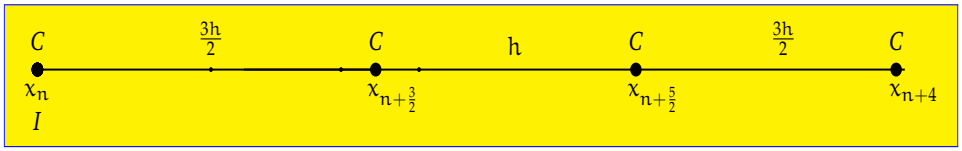

Figure 3: The classical optimal technique block figure COT2

matrix form to give

$$\begin{pmatrix} -1 & 0 & 1 & 0 & -1 \\ 0 & -1 & 0 & 3 & -\alpha \\ 0 & -1 & -2h & -3h^2+3 & -\alpha^2 h-\alpha-\frac{1}{2}\alpha^3 h^2-\frac{1}{6}\alpha^4 h^3 \\ 0 & -1 & -3h & -\frac{27}{4}h^2+3 & -\alpha-\frac{3}{2}\alpha^2 h-\frac{9}{8}\alpha^3 h^2-\frac{9}{16}\alpha^4 h^3 \\ 0 & 0 & -2 & -9h & -\alpha^2-\frac{3}{2}\alpha^3 h-\frac{9}{8}\alpha^4 h^2 \end{pmatrix} \begin{pmatrix} a_0 \\ a_1 \\ a_2 \\ a_3 \\ a_4 \end{pmatrix} = \begin{pmatrix} y_n \\ f_n \\ f_{n+1} \\ f_{n+\frac{3}{2}} \\ g_{n+\frac{3}{2}} \end{pmatrix}, \quad (3.5)$$

Equation (3.5) can be written in a compressed form as

$$XA = F, \quad (3.6)$$

where,

$$X = \begin{pmatrix} -1 & 0 & 1 & 0 & -1 \\ 0 & -1 & 0 & 3 & -\alpha \\ 0 & -1 & -2h & -3h^2+3 & -\alpha^2 h-\alpha-\frac{1}{2}\alpha^3 h^2-\frac{1}{6}\alpha^4 h^3 \\ 0 & -1 & -3h & -\frac{27}{4}h^2+3 & -\alpha-\frac{3}{2}\alpha^2 h-\frac{9}{8}\alpha^3 h^2-\frac{9}{16}\alpha^4 h^3 \\ 0 & 0 & -2 & -9h & -\alpha^2-\frac{3}{2}\alpha^3 h-\frac{9}{8}\alpha^4 h^2 \end{pmatrix}, \quad A = \begin{pmatrix} a_0 \\ a_1 \\ a_2 \\ a_3 \\ a_4 \end{pmatrix}, \quad F = \begin{pmatrix} y_n \\ f_n \\ f_{n+1} \\ f_{n+\frac{3}{2}} \\ g_{n+\frac{3}{2}} \end{pmatrix}.$$

From Equation (3.6), the matrix inverse approach is applied using MAPLE software environment and A is solved for to give

$$a_0 = y_n - \frac{(7\alpha^4 h^2-8\alpha^2-16)}{6\alpha^4 h^3} f_n + \frac{3(3\alpha^4 h^2-8\alpha^2-16)}{2\alpha^4 h^3} f_{n+1} - \frac{2(5\alpha^4 h^2-16\alpha^2-32)}{3\alpha^4 h^3} f_{n+\frac{3}{2}} + \frac{(\alpha^4 h^2-4\alpha^2-8)}{\alpha^4 h^2} g_{n+\frac{3}{2}},$$

$$a_1 = \frac{9\left(9\alpha^3h^3+16\,\alpha^3h+12\,\alpha^2+24\right)}{\alpha^3h^3}f_n - \frac{12\left(\alpha^3h+\alpha^2+2\right)}{\alpha^3h^3}f_{n+1} + \frac{4\left(23\,\alpha^3h+24\,\alpha^2+48\right)}{9\alpha^3h^3}f_{n+\frac{3}{2}} - \frac{2\left(5\,\alpha^3h+6\,\alpha^2+12\right)}{3\alpha^3h^2}g_{n+\frac{3}{2}},$$

$$a_2 = -\frac{\left(7\,\alpha^2h^2-8\right)}{6\alpha^2h^3}f_n + \frac{3\left(3\,\alpha^2h^2-8\right)}{2\alpha^2h^3}f_{n+1} - \frac{2\left(5\,\alpha^2h^2-16\right)}{3\alpha^2h^3}f_{n+\frac{3}{2}} + \frac{\left(\alpha^2h^2-4\right)}{\alpha^2h^2}g_{n+\frac{3}{2}},$$

$$a_3 = \frac{(16\,\alpha\,h+12)}{27\,\alpha\,h^3}f_n - \frac{4\,(\alpha\,h+1)}{\alpha\,h^3}f_{n+1} + \frac{(92\,\alpha\,h+96)}{27\,\alpha\,h^3}f_{n+\frac{3}{2}} - \frac{2\,(5\,\alpha\,h+6)}{9\alpha\,h^2}g_{n+\frac{3}{2}},$$

$$a_4 = -\frac{8}{3\alpha^4h^3}f_n + \frac{24}{\alpha^4h^3}f_{n+1} - \frac{64}{3\,\alpha^4h^3}f_{n+\frac{3}{2}} + \frac{8}{\alpha^4h^2}g_{n+\frac{3}{2}}.$$

The $a_j's$ are then subsituted into Equation (3.1) and after some algebraic manipulations and evaluating at $x = x_{n+\psi h}, \psi = 1$ and $\frac{3}{2}$ yields the first formula called "Classical optimal technique one (COT1)"

$$y_{n+1} = y_n + \frac{17}{54}hf_n + \frac{3}{2}hf_{n+1} - \frac{22}{27}hf_{n+\frac{3}{2}} + \frac{2}{9}h^2g_{n+\frac{3}{2}}, \tag{3.7}$$

$$y_{n+\frac{3}{2}} = y_n + \frac{5}{16}hf_n + \frac{27}{16}hf_{n+1} - \frac{1}{2}hf_{n+\frac{3}{2}} + \frac{3}{16}h^2g_{n+\frac{3}{2}}. \tag{3.8}$$

In the same manner, we generate "COT2, COT3 and COT4" as

$$y_{n+1} = y_n + \frac{7}{27}hf_n + \frac{20}{27}hf_{n+\frac{3}{2}} - \frac{1}{2}h^2g_{n+1} - \frac{1}{9}h^2g_{n+\frac{3}{2}}, \tag{3.9}$$

$$y_{n+\frac{3}{2}} = y_n + \frac{1}{4}hf_n + \frac{5}{4}hf_{n+\frac{3}{2}} - \frac{9}{16}h^2g_{n+1} - \frac{3}{16}h^2g_{n+\frac{3}{2}}, \tag{3.10}$$

$$y_{n+1} = y_n + \frac{39}{151}hf_n + \frac{112}{151}hf_{n+\frac{3}{2}} - \frac{23305}{46206}h^2g_{n+1} - \frac{2500}{23103}h^2g_{n+\frac{151}{100}}, \tag{3.11}$$

$$y_{n+\frac{3}{2}} = y_n + \frac{75}{302}hf_n + \frac{189}{151}hf_{n+\frac{3}{2}} - \frac{11703}{20536}h^2g_{n+1} - \frac{1875}{10268}h^2g_{n+\frac{151}{100}}, \tag{3.12}$$

$$y_{n+\frac{151}{100}} = y_n + \frac{372517}{1500000}hf_n + \frac{1892483}{1500000}hf_{n+\frac{3}{2}} - \frac{5449439}{9562500}h^2g_{n+1} - \frac{1117249}{6120000}h^2g_{n+\frac{151}{100}}. \tag{3.13}$$

$$y_{n+1} = y_n + \frac{877349}{3397349}hf_n + \frac{2520000}{3397349}hf_{n+\frac{151}{100}} - \frac{397700}{3442347}h^2g_{n+\frac{151}{100}} - \frac{23003}{45594}h^2g_{n+1}, \tag{3.14}$$

$$y_{n+\frac{151}{100}} = y_n + \frac{7399}{29800}hf_n + \frac{37599}{29800}hf_{n+\frac{151}{100}} - \frac{177824999}{911880000}h^2g_{n+\frac{151}{100}} - \frac{519885601}{911880000}h^2g_{n+1}. \tag{3.15}$$

We then obtain from Equations (3.7)–(3.15) by rewritten in block form

$$Q_0 Y_m = Q_1 Y_{m-1} + hQ_2 f(Y_{m-1}) + hQ_3 f(Y_m) + h^2 Q_4 g(Y_m), \tag{3.16}$$

So that Equation (3.16) yields

$$\begin{pmatrix} 1 & 0 \\ 0 & 1 \end{pmatrix} \begin{pmatrix} y_{n+1} \\ y_{n+\frac{3}{2}} \end{pmatrix} = \begin{pmatrix} 0 & 1 \\ 0 & 1 \end{pmatrix} \begin{pmatrix} y_{n-1} \\ y_n \end{pmatrix} + h \begin{pmatrix} 0 & \frac{17}{54} \\ 0 & \frac{5}{16} \end{pmatrix} \begin{pmatrix} f_{n-1} \\ f_n \end{pmatrix} + h \begin{pmatrix} \frac{3}{2} & -\frac{22}{27} \\ \frac{27}{16} & -\frac{1}{2} \end{pmatrix} \begin{pmatrix} f_{n+1} \\ f_{n+\frac{3}{2}} \end{pmatrix} + h^2 \begin{pmatrix} 0 & \frac{2}{9} \\ 0 & \frac{3}{16} \end{pmatrix} \begin{pmatrix} g_{n+1} \\ g_{n+\frac{3}{2}} \end{pmatrix}, \tag{3.17}$$

where,

$$Q_0 = \begin{pmatrix} 1 & 0 \\ 0 & 1 \end{pmatrix}, \quad Q_1 = \begin{pmatrix} 0 & 1 \\ 0 & 1 \end{pmatrix}, \quad Q_2 = \begin{pmatrix} 0 & \frac{17}{54} \\ 0 & \frac{5}{16} \end{pmatrix}, \quad Q_3 = \begin{pmatrix} \frac{3}{2} & -\frac{22}{27} \\ \frac{27}{16} & -\frac{1}{2} \end{pmatrix}, \quad Q_4 = \begin{pmatrix} 0 & \frac{2}{9} \\ 0 & \frac{3}{16} \end{pmatrix},$$

and

$$Y_m = \begin{pmatrix} y_{n+1} \\ y_{n+\frac{3}{2}} \end{pmatrix}, \quad Y_{m-1} = \begin{pmatrix} y_{n-1} \\ y_n \end{pmatrix}, \quad f(Y_{m-1}) = \begin{pmatrix} f_{n-1} \\ f_n \end{pmatrix}, \quad f(Y_m) = \begin{pmatrix} f_{n+1} \\ f_{n+\frac{3}{2}} \end{pmatrix},$$

$$g(Y_m) = \begin{pmatrix} g_{n+1} \\ g_{n+\frac{3}{2}} \end{pmatrix},$$

Again, using Equations (3.9) and (3.10), that is, COT2 in the form of Equation (3.16) yields

$$P_0 = \begin{pmatrix} 1 & 0 \\ 0 & 1 \end{pmatrix}, \quad P_1 = \begin{pmatrix} 0 & 1 \\ 0 & 1 \end{pmatrix}, \quad P_2 = \begin{pmatrix} 0 & \frac{7}{27} \\ 0 & \frac{1}{4} \end{pmatrix}, \quad P_3 = \begin{pmatrix} 0 & \frac{20}{27} \\ 0 & \frac{5}{4} \end{pmatrix}, \quad P_4 = \begin{pmatrix} -\frac{1}{2} & -\frac{1}{9} \\ -\frac{9}{16} & -\frac{3}{16} \end{pmatrix},$$

with $Y_m, Y_{m-1}, f(Y_m), f(Y_{m-1})$ and $g(Y_m)$ defined above respectively.

So that, by resolving Equations (3.11)–(3.13), that is, COT3 in the form of Equation (3.16) gives

$$R_0 = \begin{pmatrix} 1 & 0 \\ 0 & 1 \end{pmatrix}, R_1 = \begin{pmatrix} 0 & 1 \\ 0 & 1 \end{pmatrix}, R_2 = \begin{pmatrix} 0 & \frac{39}{151} \\ 0 & \frac{75}{302} \\ 0 & \frac{372517}{1500000} \end{pmatrix}, R_3 = \begin{pmatrix} 0 & \frac{112}{151} & 0 \\ 0 & \frac{189}{151} & 0 \\ 0 & \frac{1892483}{1500000} & 0 \end{pmatrix},$$

$$R_4 = \begin{pmatrix} -\frac{23305}{46206} & 0 & -\frac{2500}{23103} \\ -\frac{11703}{20536} & 0 & -\frac{1875}{10268} \\ -\frac{5449439}{9562500} & 0 & -\frac{1117249}{6120000} \end{pmatrix}, g(Y_m) = \begin{pmatrix} g_{n+1} \\ g_{n+\frac{3}{2}} \\ g_{n+\frac{151}{100}} \end{pmatrix}.$$

Finally, rewritten Equations (3.14) and (3.15) also, in the form Equation (3.16) produces

$$K_0 = \begin{pmatrix} 1 & 0 \\ 0 & 1 \end{pmatrix}, K_1 = \begin{pmatrix} 0 & 1 \\ 0 & 1 \end{pmatrix}, K_2 = \begin{pmatrix} 0 & \frac{877349}{3397349} \\ 0 & \frac{7399}{29800} \end{pmatrix}, K_3 = \begin{pmatrix} 0 & \frac{2520000}{3397349} \\ 0 & \frac{37599}{29800} \end{pmatrix},$$

$$K_4 = \begin{pmatrix} -\frac{23003}{45594} & -\frac{397700}{3442347} \\ -\frac{519885601}{911880000} & -\frac{177824999}{911880000} \end{pmatrix}, f(Y_m) = \begin{pmatrix} f_{n+1} \\ f_{n+\frac{151}{100}} \end{pmatrix}, g(Y_m) = \begin{pmatrix} g_{n+1} \\ g_{n+\frac{151}{100}} \end{pmatrix}.$$

4. Numerical analysis of COT1, COT2, COT3 and COT4

The analysis of the numerical properties of the proposed formulas as algebraic order, consistency, zero-stability, A-stability and convergence, are verified below.

Definition 4.1. ***Algebraic order of convergence***
Going by definition, the proposed classical optimal approaches in Equations (3.9)–(3.15), together with their linked linear operator, are taken to be of order p, provided $e_0 = e_1 = e_2 = e_3 = e_4 \ldots = e_p = 0$, $e_{p+1} \neq 0$. Given the global component, e_{p+1}, is called the error constants for the intended formulas. Therefore, define the linked operator with the proposed methods as

$$L(y(x); h) = -E^0 Y_m + E^1 Y_{m-1} + E^2 F_{m-1} + E^3 F_m + E^4 G_m, \tag{4.1}$$

given that,

$$Y_m = \begin{pmatrix} y_{n+1} \\ y_{n+\frac{3}{2}} \end{pmatrix}, Y_{m-1} = \begin{pmatrix} y_{n-1} \\ y_n \end{pmatrix}, F_{m-1} = \begin{pmatrix} f_{n-1} \\ f_n \end{pmatrix}, F_m = \begin{pmatrix} f_{n+1} \\ f_{n+\frac{3}{2}} \end{pmatrix}, \text{ as in COT1.}$$

Generally, taking into consideration the order of methods gives,

$$\left.\begin{aligned} c_0 = \sum_{j=0}^{k} \alpha_j = 0, \\ c_1 = \sum_{j=0}^{k} (j\alpha_j - \beta_j) = 0, \\ \vdots \\ c_p = \sum_{j=0}^{k} (\tfrac{1}{p!} j^p \alpha_j - \tfrac{1}{(1-p)!} j^{j-1} \beta_j) = 0,\ p = 2(1)q + 1. \end{aligned}\right\} \tag{4.2}$$

Taking the Taylor series expansion of Equations (3.9) and (3.10) using Maple software package and coefficients in powers of h, $y(x)$ and $y'(x)$ gives the order for COT1

$$c_0 = \begin{pmatrix} 1 - 1 \\ 1 - 1 \end{pmatrix} = \begin{pmatrix} 0 \\ 0 \end{pmatrix},$$

$$c_1 = \begin{pmatrix} 1 - \frac{17}{54} - \frac{3}{2} + \frac{22}{27} + 0 \\ \frac{3}{2} - \frac{5}{16} - \frac{27}{16} + \frac{1}{2} + 0 \end{pmatrix} = \begin{pmatrix} 0 \\ 0 \end{pmatrix},$$

$$c_2 = \begin{pmatrix} \frac{1}{2} + 0 - \frac{3}{2} + \frac{11}{9} - \frac{2}{9} \\ \frac{9}{8} + 0 - \frac{27}{16} + \frac{3}{4} - \frac{3}{16} \end{pmatrix} = \begin{pmatrix} 0 \\ 0 \end{pmatrix},$$

$$c_3 = \begin{pmatrix} \frac{1}{6} + 0 - \frac{3}{4} + \frac{11}{12} - \frac{1}{3} \\ \frac{9}{16} + 0 - \frac{27}{32} + \frac{9}{16} - \frac{9}{32} \end{pmatrix} = \begin{pmatrix} 0 \\ 0 \end{pmatrix},$$

$$c_4 = \begin{pmatrix} \frac{1}{24} + 0 - \frac{1}{4} + \frac{11}{24} - \frac{1}{4} \\ \frac{27}{128} + 0 - \frac{9}{32} + \frac{9}{32} - \frac{27}{128} \end{pmatrix} = \begin{pmatrix} 0 \\ 0 \end{pmatrix},$$

$$c_5 = \begin{pmatrix} \frac{1}{120} + 0 - \frac{1}{16} + \frac{11}{64} - \frac{1}{8} \\ \frac{81}{1280} + 0 - \frac{9}{128} + \frac{27}{256} - \frac{27}{256} \end{pmatrix} = \begin{pmatrix} \frac{-7}{960} \\ \frac{-9}{1280} \end{pmatrix}.$$

Therefore, COT1 is of an algebraic order of convergence of 4, since it has error constants,

$c_{p+1} = \begin{pmatrix} \frac{-7}{960} \\ \frac{-9}{1280} \end{pmatrix}$.

Similarly, for COT2, we get

$$c_0 = \begin{pmatrix} 1 - 1 \\ 1 - 1 \end{pmatrix} = \begin{pmatrix} 0 \\ 0 \end{pmatrix},$$

$$c_1 = \begin{pmatrix} 1 - \frac{7}{27} - \frac{20}{27} + 0 + 0 \\ \frac{3}{2} - \frac{1}{4} - \frac{5}{4} + 0 + 0 \end{pmatrix} = \begin{pmatrix} 0 \\ 0 \end{pmatrix},$$

$$c_2 = \begin{pmatrix} \frac{1}{2} + 0 - \frac{10}{9} + \frac{1}{2} + \frac{1}{9} \\ \frac{9}{8} + 0 - \frac{15}{8} + \frac{9}{16} + \frac{3}{16} \end{pmatrix} = \begin{pmatrix} 0 \\ 0 \end{pmatrix},$$

$$c_3 = \begin{pmatrix} \frac{1}{6} + 0 - \frac{5}{6} + \frac{1}{2} + \frac{1}{6} \\ \frac{9}{16} + 0 - \frac{45}{32} + \frac{9}{16} + \frac{9}{32} \end{pmatrix} = \begin{pmatrix} 0 \\ 0 \end{pmatrix},$$

$$c_4 = \begin{pmatrix} \frac{1}{24} + 0 - \frac{5}{12} + \frac{1}{4} + \frac{1}{8} \\ \frac{27}{128} + 0 - \frac{45}{64} + \frac{9}{32} + \frac{27}{128} \end{pmatrix} = \begin{pmatrix} 0 \\ 0 \end{pmatrix},$$

$$c_5 = \begin{pmatrix} \frac{1}{120} + 0 - \frac{5}{32} + \frac{1}{12} + \frac{1}{16} \\ \frac{81}{1280} + 0 - \frac{135}{512} + \frac{3}{32} + \frac{27}{256} \end{pmatrix} = \begin{pmatrix} -\frac{1}{480} \\ -\frac{3}{2560} \end{pmatrix}.$$

Again, COT2 is confirmed to have an algebraic order of convergence of 4 since $c_{p+1} = \begin{pmatrix} -\frac{1}{480} \\ -\frac{3}{2560} \end{pmatrix}$.

With the same approach, the algebraic order of convergence of COT3 and COT4 are found to be 4 each with the error constants

$$c_{p+1} = \begin{pmatrix} -\frac{713}{362400} \\ -\frac{1887}{1932800} \\ \frac{-48816941}{50000000000} \end{pmatrix}, \qquad c_{p+1} = \begin{pmatrix} -\frac{8777}{4470000} \\ \frac{-346763695867}{357600000000000} \end{pmatrix}.$$

4.1. *Zero-stability* [26]

The zero-stabilty property plays crucial roles in the use of numerical methods to approximate the true behaviour of dynamic system(s). Within the integration interval, it ensures

that the approximate solutions of a method are put under check so that its solutions are bounded as iterations proceed for any perturbation on the initial conditions. More practically, the zero stability controls errors committed at each stage of iterations, which is usually, referred to as "the local truncation error (LTE)" and as well as, errors evolved in the entire iterations, simply called "the global truncation error (GTE)", such that they do not diverge from the true solution of the system.
Therefore, the zero stability of the suggested formulas are verified through a test equation approach.

Definition 4.2. ***The zero-stability of COT1, COT2, COT3 and COT4***
The derived methods in Equations (3.7)–(3.15) are said to be zero-stable if no root of the first characteristic polynomial has modulus greater than one and that every root with modulus one is simple. That is, no zero of the charateristic polynomial that is one, has multiplicity. Therefore, substitute the scalar test equation, $y^i = (\lambda y)^i, i = 1(1)$, into the intended formulas to obtain

$$\left.\begin{aligned} y_{n+1} &= y_n + \frac{17}{54}h\lambda y_n + \frac{3}{2}h\lambda y_{n+1} - \frac{22}{27}h\lambda y_{n+\frac{3}{2}} + \frac{2}{9}h^2\lambda^2 y^2_{n+\frac{3}{2}}, \\ y_{n+\frac{3}{2}} &= y_n + \frac{5}{16}h\lambda y_n + \frac{27}{16}h\lambda y_{n+1} - \frac{1}{2}h\lambda y_{n+\frac{3}{2}} + \frac{3}{16}h^2\lambda^2 y^2_{n+\frac{3}{2}}. \end{aligned}\right\} \tag{4.3}$$

Equation (4.3) can be rewritten in a compact matrix form to produce

$$\begin{pmatrix} 1 & 0 \\ 0 & 1 \end{pmatrix}\begin{pmatrix} y_{n+1} \\ y_{n+\frac{3}{2}} \end{pmatrix} = \begin{pmatrix} 0 & 1 \\ 0 & 1 \end{pmatrix}\begin{pmatrix} y_{n-1} \\ y_n \end{pmatrix} + \begin{pmatrix} 0 & \frac{17}{54} \\ 0 & \frac{5}{16} \end{pmatrix}\begin{pmatrix} h\lambda y_{n-1} \\ h\lambda y_n \end{pmatrix} + \begin{pmatrix} \frac{3}{2} & -\frac{22}{27} \\ \frac{27}{16} & -\frac{1}{2} \end{pmatrix}\begin{pmatrix} h\lambda y_{n+1} \\ h\lambda y_{n+\frac{3}{2}} \end{pmatrix} + \begin{pmatrix} 0 & \frac{2}{9} \\ 0 & \frac{3}{16} \end{pmatrix}\begin{pmatrix} h^2\lambda^2 y^2_{n+1} \\ h^2\lambda^2 y_{n+\frac{3}{2}} \end{pmatrix}, \tag{4.4}$$

So that Equation (4.4) yields

$$R = P_0 w - (P_1 + zP_2 + zP_3 w + z^2 P_4 w). \tag{4.5}$$

with $z = \lambda h$ and $w = y^i_{n+\tau}, i = 1(1), \tau = 1, \frac{3}{2}, \frac{151}{100}$, is the difference shift operator with λ assumed to go through the Jacobian negative eigenvalues. Simplifying Equation (4.5) gives

$$R = \begin{pmatrix} w - \frac{3}{2}wz & -1 - \frac{17}{54}z + \frac{22}{27}wz - \frac{2}{9}wz^2 \\ -\frac{27}{16}wz & w - 1 - \frac{5}{16}z + \frac{1}{2}wz - \frac{3}{16}wz^2 \end{pmatrix} \tag{4.6}$$

The determinant of Equation (4.6) is then taken to produce the stability polynomial

$$D_1(z, w) = w^2 - w - \frac{1}{2}wz - w^2 z + \frac{7}{16}w^2 z^2 - \frac{1}{16}wz^2 - \frac{3}{32}w^2 z^3. \tag{4.7}$$

For COT2, we have the following after the test equation substitution

$$\left.\begin{aligned} y_{n+1} &= y_n + \frac{7}{27}h\lambda y_n + \frac{20}{27}h\lambda y_{n+\frac{3}{2}} - \frac{1}{2}h^2\lambda^2 y^2_{n+1} - \frac{1}{9}h^2\lambda^2 y^2_{n+\frac{3}{2}},\\ y_{n+\frac{3}{2}} &= y_n + \frac{1}{4}h\lambda y_n + \frac{5}{4}h\lambda y_{n+\frac{3}{2}} - \frac{9}{16}h^2\lambda^2 y^2_{n+1} - \frac{3}{16}h^2\lambda^2 y^2_{n+\frac{3}{2}} \end{aligned}\right\} \tag{4.8}$$

Put Equation (4.8) in the form of Equations (4.4)–(4.7) gives the stability polynomial for COT2

$$D_2(z,w) = w^2 - w - \frac{1}{4}wz - \frac{5}{4}w^2z + \frac{11}{16}w^2z^2 + \frac{1}{16}wz^2 + \frac{1}{48}wz^3 - \frac{5}{24}w^2z^3 + \frac{1}{32}w^2z^4. \tag{4.9}$$

Again, COT3 can be put in the form

$$\left.\begin{aligned} y_{n+1} &= y_n + \frac{39}{151}h\lambda y_n + \frac{112}{151}h\lambda y_{n+\frac{3}{2}} - \frac{23305}{46206}h^2\lambda^2 y^2_{n+1} - \frac{2500}{23103}h^2\lambda^2 y^2_{n+\frac{151}{100}},\\ y_{n+\frac{3}{2}} &= y_n + \frac{75}{302}h\lambda y_n + \frac{189}{151}h\lambda y_{n+\frac{3}{2}} - \frac{11703}{20536}h^2\lambda^2 y_{n+1} - \frac{1875}{10268}h^2\lambda^2 y_{n+\frac{151}{100}},\\ y_{n+\frac{151}{100}} &= y_n + \frac{372517}{1500000}h\lambda y_n + \frac{1892483}{1500000}h\lambda y_{n+\frac{3}{2}} - \frac{5449439}{9562500}h^2\lambda^2 y^2_{n+1}\\ &\quad - \frac{1117249}{6120000}h^2\lambda^2 y_{n+\frac{151}{100}}. \end{aligned}\right\} \tag{4.10}$$

Resolve Equation (4.10) in the form of Equations (4.4)–(4.7) to give also the stability polynomial for COT3

$$D_3(z,w) = w^3 - w^2 - \frac{3901}{15100}w^2z + \frac{12447149}{18120000}w^3z^2 - \frac{189}{151}w^3z + \frac{228389}{3624000}w^2z^2 - \frac{2497199}{12080000}w^3z^3 + \frac{40922549}{1812000000}w^2z^3 + \frac{4379\,w^3z^4}{144000} + \frac{7903}{36000000}w^2z^4 + \frac{151}{480000}w^3z^5. \tag{4.11}$$

Finally, for COT4, after substitution of the test equation yields

$$\left.\begin{aligned} y_{n+1} &= y_n\frac{877349}{3397349}h\lambda y_n + \frac{2520000}{3397349}h\lambda y_{n+\frac{151}{100}} - \frac{397700}{3442347}h^2\lambda^2 y^2_{n+\frac{151}{100}}\\ &\quad - \frac{23003}{45594}h^2\lambda^2 y^2_{n+1},\\ y_{n+\frac{151}{100}} &= y_n + \frac{7399}{29800}h\lambda y_n + \frac{37599}{29800}h\lambda y_{n+\frac{151}{100}} - \frac{177824999}{911880000}h^2\lambda^2 y^2_{n+\frac{151}{100}}\\ &\quad - \frac{519885601}{911880000}h^2\lambda^2 y^2_{n+1}. \end{aligned}\right\} \tag{4.12}$$

Equation (4.12) is then resolved in the form of Equations (4.4)–(4.7) to produce the stability polynomial for COT4

$$D_4(z,w) = w^2 - w - \frac{7399}{29800}wz - \frac{37599}{29800}w^2z + \frac{4169183}{5960000}w^2z^2 + \frac{391017}{5960000}wz^2 + \frac{130917}{5960000}wz^3 - \frac{38203}{178800}w^2z^3 + \frac{387617}{11920000}w^2z^4. \tag{4.13}$$

Therefore, set $z = 0$ in Equations (4.7), (4.9), (4.11) and (4.13), equate each to zero and solve for w to give the zeros of the equations as $w = 0, 1$ each, indicating that COT1, COT2, COT4 and $w = 0, 0, 1$ for COT3 are zero stable, since $w \leqslant 1$, according to Definition 4.2.

4.2. Consistency [26]

Lemma 1. *The consistency of methods*
The unique schemes in Equations (3.7)–(3.15) are consistent if and only if the following conditions are satisfied,

i that the order, $p \geqslant 1$,

ii that $\sum_{j=0} \alpha_j = 0$,

iii that $\sum_{j=0} j\alpha_j = \sum_{j=0} \beta_j$,

iv that $\rho'(1) = \Phi(1)$.

Since the proposed techniques have order 4 each and that $p \geqslant 1$, Item i is verified. For Item ii, a clear observation from COT1 gives $\alpha_0 = -1$ and $\alpha_1 = 1$, $\beta_0 = \frac{17}{54}, \beta_1 = \frac{3}{2}, \beta_2 = -\frac{22}{27}$. From the foregoing, it is clear that $\sum_{j=0}^{1} j\alpha_j = \sum_{j=0}^{2} \beta_j = 1$, is satisfied in Item iii. Again, from COT1, $\rho(t) = t$ and $\phi(t) = \frac{17}{54} + \frac{3}{2}t - \frac{22}{27}t^{\frac{3}{2}}$, so that $\rho'(1) = \phi(1) = 1$. Thus, Item iv is confirmed. Hence, COT1 is a consistent method since Lemma 1 condtions are satified. Obviously, for COT2, Item i is satisfied since $p \geqslant 1$. For $\alpha_0 = -1$ and $\alpha_1 = 1$ confirms Item ii also.
Investigation from Item iii when $\beta_0 = \frac{7}{27}$ and $\beta_1 = \frac{20}{27}$ reveals that $\sum_{j=0}^{1} j\alpha_j = \sum_{j=0}^{2} \beta_j = 1$, therefore, Item iii is verified. Also, for Item iv, $\rho(t) = t$ and $\phi(t) = \frac{7}{27} + \frac{20}{27}t^{\frac{3}{2}}$ and that $\rho'(1) = \phi(1) = 1$, showing that it is satisifed also. In the same way, COT3 and COT4 are true for Lemma 1.

4.3. Convergence

Theorem 4.1. *The convergence of methods*
Inline with [26], consistency and zero-stability are the necessary and sufficient conditions for every numerical methods to be convergent. Therefore, since the proposed schemes are both zero-stable and consistent, they are certainly convergent.

4.4. Absolute stability region

The absolute stability is another critical feature that depicts the short-term and long-term behaviour of a dynamic system. In structural engineering, it is used to investigate structural stability over a short and distant time. For a numerical method, it should be able to provide acceptable solutions given any perturbation on the initial conditions, otherwise

the formula is said to be unstable. Therefore, a numerical formula is said to be absolutely stable if the whole of the left-half plane $z : D(z,w) \leqslant 0$ is contained in the region $z : D(z,w) \leqslant 1$. Where $D(z,w)$ is the stability polynomial of the proposed method. Therefore, the stability polynomials in Equations (4.7), (4.9), (4.11) and (4.13) are then coded on MATLAB R2023a to yield the absolute stability plots below.

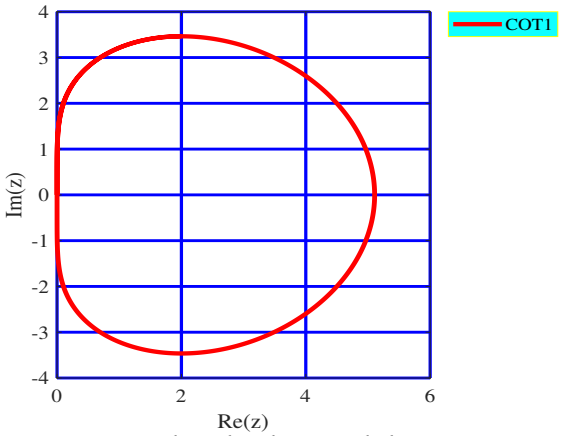

Figure 4: The absolute stability region of COT1

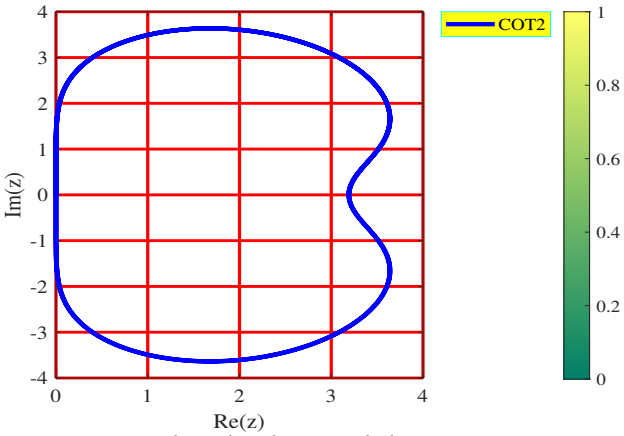

Figure 5: The absolute stability region of COT2

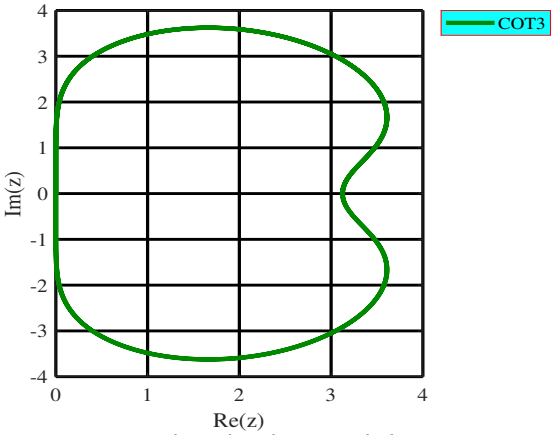

Figure 6: The absolute stability region of COT3

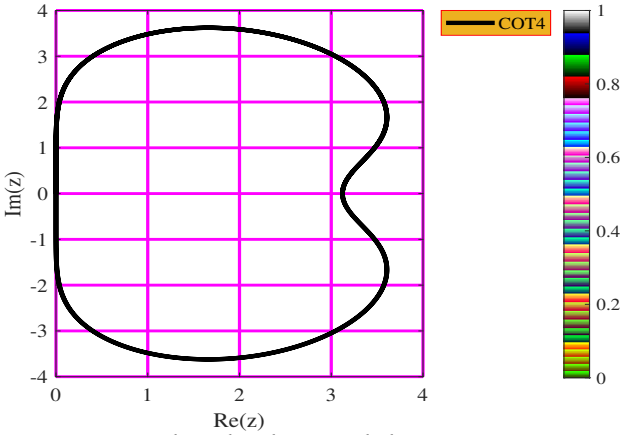

Figure 7: The absolute stability region of COT4

Definition 4.3. *Orthogonal polynomials* [27]
A system of polynomials $f_n(x)$, degree $[f_n(x)] = n$, is called orthogonal on the interval $a \leqslant x \leqslant b$, with respect to the weight function $w(x)$, if $\int_a^b w(x)f_n(x)f_m(x) = 0, \quad (n \neq m; n, m = 0(1))$. The weight function $w(x)$, where $(w(x) \geqslant 0)$ determines the system $f_n(x)$ up to a constant factor in each polynomial. The specification of these factors is referred to as standardization.

Definition 4.4. *ξ-stable* [26]
If the roots $\xi_k(h\lambda)$ of the characteristic equation corresponding to the multi-derivative

formula satisfy for some finite k,
$|h\lambda| < \max_i^n\{|\xi_i(h\lambda)|\} < k, \quad \forall\ n \leqslant \xi$ as $h\lambda \to -\infty$, then the method is $\xi-$stable.

A sufficient but not necessary condition for a method to be stable at infinity is that the method is $\xi-$stable for $\xi > 0$. From Figures 4–7, it is clear that, the proposed methods are certainly A-stable.

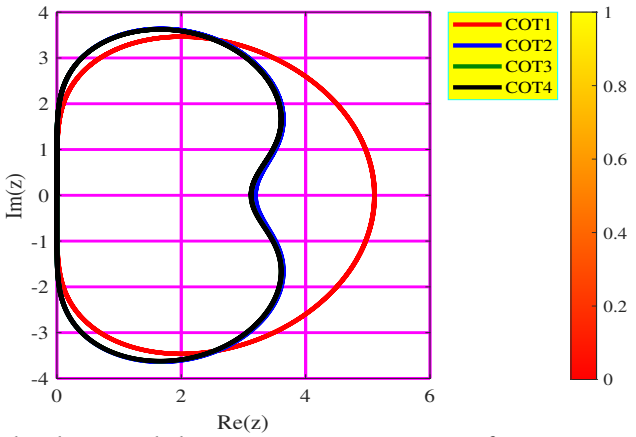

Figure 8: The absolute stability region comparison for COT1, COT2, COT3 and COT4

5. Implementation procedures of methods

The traditional techniques of Newton Raphson's method is used for the implementation of COT1, COT2, COT3 and COT4. Therefore, let $y_{n+1}^{(i+1)}$, $y_{n+\frac{3}{2}}^{(i+1)}$ and $y_{n+\frac{151}{100}}^{(i+1)}$ represent the $(i+1)^{th}$ iterative values for y_{n+1}, $y_{n+\frac{3}{2}}$ and $y_{n+\frac{151}{100}}$ respectively. While the major drawbacks of the proposed techniques is in the provision of an additional derivative function that are required in the formulation and iteration processes, including the dynamic structure in the collocation part, advantages abound and that methods converge fast with high accuracy and precision factor.
By applying Newton's iteration procedures to Equations (3.7)–(3.15), $y_{n+1}^{(i+1)}$, $y_{n+\frac{3}{2}}^{(i+1)}$ and $y_{n+\frac{151}{100}}^{(i+1)}$ are obtained. The proceedures take the form

$$\begin{aligned}
y_{n+1}^{(i+1)} &= y_{n+1}^{(i)} - \frac{F_1\left(y_{n+1}^{(i)}\right)}{F_1'\left(y_{n+1}^{(i)}\right)}, \\
y_{n+\frac{3}{2}}^{(i+1)} &= y_{n+\frac{3}{2}}^{(i)} - \frac{F_2\left(y_{n+\frac{3}{2}}^{(i)}\right)}{F_2'\left(y_{n+\frac{3}{2}}^{(i)}\right)}, \\
y_{n+\frac{151}{100}}^{(i+1)} &= y_{n+\frac{151}{100}}^{(i)} - \frac{F_3\left(y_{n+\frac{151}{100}}^{(i)}\right)}{F_3'\left(y_{n+\frac{151}{100}}^{(i)}\right)},
\end{aligned} \tag{5.1}$$

where, for COT1

$$F_1(y_{n+1}^{(i)}) = y_{n+1}^{(i)} - y_n^{(i)} - \tfrac{17}{54}hf_n^{(i)} - \tfrac{3}{2}hf_{n+1}^{(i)} + \tfrac{22}{27}hf_{n+\frac{3}{2}}^{(i)} - \tfrac{2}{9}h^2g_{n+\frac{3}{2}}^{(i)},$$

$$F_2(y_{n+\frac{3}{2}}^{(i)}) = y_{n+\frac{3}{2}}^{(i)} - y_n^{(i)} - \tfrac{5}{16}hf_n^{(i)} - \tfrac{27}{16}hf_{n+1}^{(i)} + \tfrac{1}{2}hf_{n+\frac{3}{2}}^{(i)} - \tfrac{3}{16}h^2g_{n+\frac{3}{2}}^{(i)},$$

and that

$$F_1'(y_{n+1}^{(i)}) = 1 - \tfrac{3}{2}h\frac{\partial f_{n+1}}{\partial y_{n+1}},$$

$$F_2'(y_{n+\frac{3}{2}}^{(i)}) = 1 + \tfrac{1}{2}h\frac{\partial f_{n+\frac{3}{2}}}{\partial y_{n+\frac{3}{2}}} - \tfrac{3}{16}h^2\frac{\partial g_{n+\frac{3}{2}}}{\partial y_{n+\frac{3}{2}}},$$

After substitution of above into Equation (5.1), we get

$$y_{n+1}^{(i+1)} - y_{n+1}^{(i)} = -\frac{\left(y_{n+1}^{(i)} - y_n^{(i)} - \frac{17}{54}hf_n^{(i)} - \frac{3}{2}hf_{n+1}^{(i)} + \frac{22}{27}hf_{n+\frac{3}{2}}^{(i)} - \frac{2}{9}h^2g_{n+\frac{3}{2}}^{(i)}\right)}{\left(1 - \frac{3}{2}h\frac{\partial f_{n+1}}{\partial y_{n+1}}\right)}, \tag{5.2}$$

$$y_{n+\frac{3}{2}}^{(i+1)} - y_{n+\frac{3}{2}}^{(i)} = -\frac{\left(y_{n+\frac{3}{2}}^{(i)} - y_n^{(i)} - \frac{5}{16}hf_n^{(i)} - \frac{27}{16}hf_{n+1}^{(i)} + \frac{1}{2}hf_{n+\frac{3}{2}}^{(i)} - \frac{3}{16}h^2g_{n+\frac{3}{2}}^{(i)}\right)}{\left(1 + \frac{1}{2}h\frac{\partial f_{n+\frac{3}{2}}}{\partial y_{n+\frac{3}{2}}} - \frac{3}{16}h^2\frac{\partial g_{n+\frac{3}{2}}}{\partial y_{n+\frac{3}{2}}}\right)}, \tag{5.3}$$

Simplifying further Equations (5.2) and (5.3) produce

$$\left(y_{n+1}^{(i+1)} - y_{n+1}^{(i)}\right)\left(1 - \frac{3}{2}h\frac{\partial f_{n+1}}{\partial y_{n+1}}\right) = -\left(y_{n+1}^{(i)} - y_n^{(i)} - \frac{17}{54}hf_n^{(i)} - \frac{3}{2}hf_{n+1}^{(i)} + \frac{22}{27}hf_{n+\frac{3}{2}}^{(i)} - \frac{2}{9}h^2g_{n+\frac{3}{2}}^{(i)}\right), \tag{5.4}$$

$$\left(y_{n+\frac{3}{2}}^{(i+1)} - y_{n+\frac{3}{2}}^{(i)}\right)\left(1 + \frac{1}{2}h\frac{\partial f_{n+\frac{3}{2}}}{\partial y_{n+\frac{3}{2}}} - \frac{3}{16}h^2\frac{\partial g_{n+\frac{3}{2}}}{\partial y_{n+\frac{3}{2}}}\right) = -\left(y_{n+\frac{3}{2}}^{(i)} - y_n^{(i)} - \frac{5}{16}hf_n^{(i)} - \frac{27}{16}hf_{n+1}^{(i)} + \frac{1}{2}hf_{n+\frac{3}{2}}^{(i)} - \frac{3}{16}h^2g_{n+\frac{3}{2}}^{(i)}\right), \tag{5.5}$$

If we let $e_{n+1}^{(i+1)} = y_{n+1}^{i+1} - y_{n+1}^{i}$ and $e_{n+\frac{3}{2}}^{(i+1)} = y_{n+\frac{3}{2}}^{i+1} - y_{n+\frac{3}{2}}^{i}$, Equations (5.4) and (5.5) become

$$e_{n+1}^{(i+1)}\left(1 - \frac{3}{2}h\frac{\partial f_{n+1}}{\partial y_{n+1}}\right) = -\left(y_{n+1}^{(i)} - y_n^{(i)} - \frac{17}{54}hf_n^{(i)} - \frac{3}{2}hf_{n+1}^{(i)} + \frac{22}{27}hf_{n+\frac{3}{2}}^{(i)} - \frac{2}{9}h^2g_{n+\frac{3}{2}}^{(i)}\right), \tag{5.6}$$

$$e_{n+\frac{3}{2}}^{(i+1)}\left(1 + \frac{1}{2}h\frac{\partial f_{n+\frac{3}{2}}}{\partial y_{n+\frac{3}{2}}} - \frac{3}{16}h^2\frac{\partial g_{n+\frac{3}{2}}}{\partial y_{n+\frac{3}{2}}}\right) = -\left(y_{n+\frac{3}{2}}^{(i)} - y_n^{(i)} - \frac{5}{16}hf_n^{(i)} - \frac{27}{16}hf_{n+1}^{(i)} + \frac{1}{2}hf_{n+\frac{3}{2}}^{(i)} - \frac{3}{16}h^2g_{n+\frac{3}{2}}^{(i)}\right), \tag{5.7}$$

Therefore, the approximate solutions to $y_{n+1}^{(i+1)}$ and $y_{n+\frac{3}{2}}^{(i+1)}$ are

$$y_{n+1}^{(i+1)} = y_{n+1}^{(i)} - \frac{\left(y_{n+1}^{(i)} - y_n^{(i)} - \frac{17}{54}hf_n^{(i)} - \frac{3}{2}hf_{n+1}^{(i)} + \frac{22}{27}hf_{n+\frac{3}{2}}^{(i)} - \frac{2}{9}h^2g_{n+\frac{3}{2}}^{(i)}\right)}{\left(1 - \frac{3}{2}h\frac{\partial f_{n+1}}{\partial y_{n+1}}\right)}, \tag{5.8}$$

$$y_{n+\frac{3}{2}}^{(i+1)} = y_{n+\frac{3}{2}}^{(i)} - \frac{\left(y_{n+\frac{3}{2}}^{(i)} - y_n^{(i)} - \frac{5}{16}hf_n^{(i)} - \frac{27}{16}hf_{n+1}^{(i)} + \frac{1}{2}hf_{n+\frac{3}{2}}^{(i)} - \frac{3}{16}h^2g_{n+\frac{3}{2}}^{(i)}\right)}{\left(1 + \frac{1}{2}h\frac{\partial f_{n+\frac{3}{2}}}{\partial y_{n+\frac{3}{2}}} - \frac{3}{16}h^2\frac{\partial g_{n+\frac{3}{2}}}{\partial y_{n+\frac{3}{2}}}\right)}. \tag{5.9}$$

Remark: The Maple 18, MATLAB 2023a and LaTeX software environments, which are installed on a personal computer powered by Windows OS with Intel(R) Core(TM) i5-6300U CPU @ 2.40GHz 2.50GHz processor with 8.0GB RAM are used for the formulation and analysis of methods, numerical iterations, graphs plot and typesetting.

6. The numerical simulations using the proposed methods

This section presents the simulations of the intended techniques given in Equations (3.7)–(3.15) through the accuracy distributions, absolute errors$= \|y(x_n) - y_n\|$, absolute maximum error within integration interval $= Max_{1\leqslant n\leqslant N}\|y(x_n) - y_n\|$, norm $= \sqrt{\sum_{1\leqslant n\leqslant N}(y(x_n) - y_n)^2}$ and root mean square $= \sqrt{\frac{1}{N}\sum_{1\leqslant n\leqslant N}(y(x_n) - y_n)^2}$, precision factor, scd $= -\lg_{10}\|y(x_n) - y_n\|$ and the time efficiency of methods (CPU time in seconds). The integration interval is $[x_0, x_N]$. The approximation at y_n is achieved through the starting-value x_n. This is used to compute the next value for y_{n+1} at the mesh x_{n+1} and finally, the former approximate solution is then used to find $y_{n+\frac{3}{2}}$ at the discretized mesh-point $x_{n+\frac{3}{2}}$.

Problem 6.1. ***Biomass transfer in trees solved by*** **Abuasbeh *et al.* [24]**

Take, for example, a forest in Europe that only has one or two different kinds of trees.We begin by selecting some of the oldest trees, those that are forecast to pass away during the next several years, and then we trace the progression of live trees into dead ones. The dead trees will gradually rot and collapse due to the various biological and seasonal occurrences. In the end, the trees that have fallen form humus. Define the variables x, y, z, and t by the following:
$y_1(x) =$ equals the biomass that has decomposed into humus;
$y_2(x) =$ represents the biomass of dead trees;
$y_3(x) =$ represents the biomass of live trees;
$x =$ equals the amount of time in decades (one decade equals ten years).
The above practical scenerio can be then modeled into a first-order differential system of the form:

$$\begin{aligned} y_1'(x) &= -y_1(x) + 3y_2(x), \qquad y_1(0) = 0, \\ y_2'(x) &= -3y_2(x) + 5y_3(x), \qquad y_2(0) = 0, \\ y_3'(x) &= -5y_3(x), \qquad y_3(0) = 1. \end{aligned}$$

over the integration interval $[0, 10]$. Therefore, the exact solution for the model is:

$$y_1(x) = \frac{15}{8}e^{-5x}(-1 + e^{2x})^2,$$
$$y_2(x) = \frac{5}{2}e^{-5x}(-1 + e^{2x}),$$
$$y_3(x) = e^{-5x}.$$

The results from simulating Problem 6.1 are shown in Tables 1–3. Figure 9 is the exact surface function plots showing inter-connected dynamic differential system. It clearly shows that it could provide acceptable solutions given satisfied starting values with good stable methods (whose approximations are bounded over the integration interval $[a, b]$). The Problem 6.1 is a special application problem from the life-cycle of trees over some periods of time. It is called "biomass transfer in trees". This particular problem has been solved taking into consideration different accuracy distributions, ranging from infinity norm, the root mean square at the end of integration interval, the mean and precision factor at varied step number and sizes. The results and solution plots from dsolve in MAPLE are displayed in Tables 1–3 and Figures 10–12. Figures 13–23 depict the accuracy curves comparing the approximate with true solutions. While a clear observation of the foregoing figures presents convincing agreement from dsolve package in MAPLE and proposed formulas, the tables also give improved accuracy and high precision factors in COT1, COT2, COT3 and COT4, with COT4 outperformed the remaining methods. A clear comparison of the suggested methods with NPOBM of order 4 in Abuasbeh *et al.* [24] presents improved accuracy.

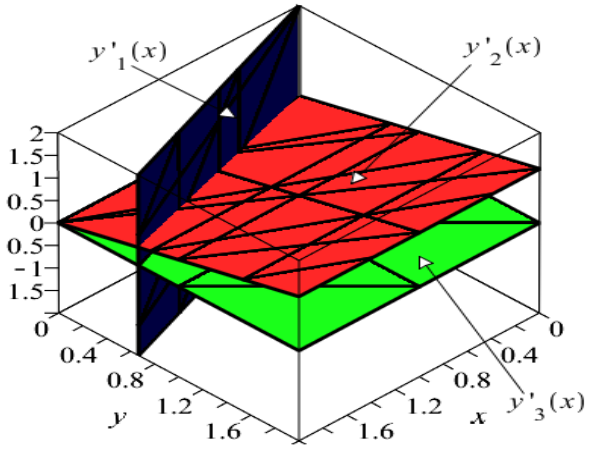

Figure 9: The function plots showing physically connected differential systems for Problem 6.1

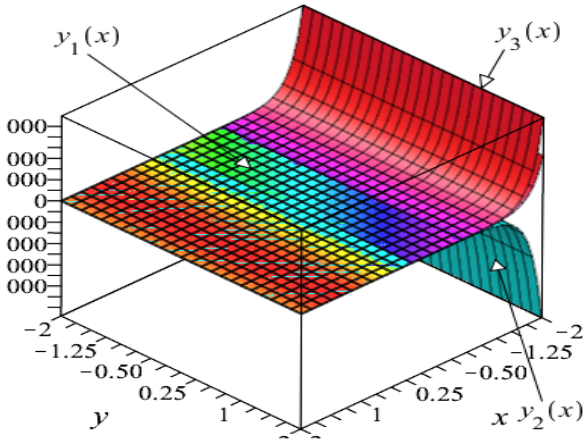

Figure 10: The exact function plots showing connected surface functions for Problem 6.1

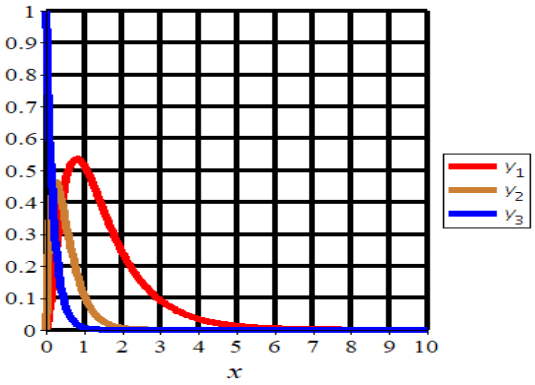

Figure 11: The MAPLE dsolve plots using the embedded Gear's method for Problem 6.1 when NS $= 2^6$

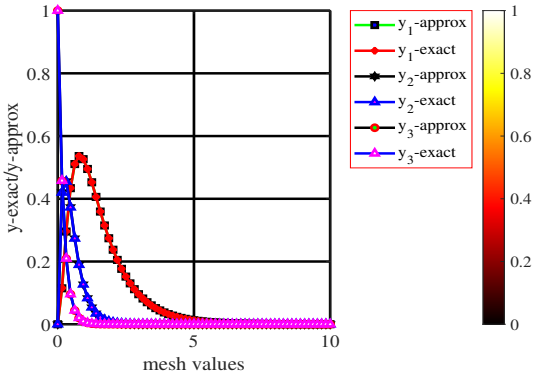

Figure 12: The accuracy curves of Problem 6.1 when NS $= 2^6$ for COT1

Table 1: The results for Problem 6.1 with N $= 2^6$ where x $\in [0, 10]$

Methods	Norm$_\infty$	RMSE	Mean	scd
COT1, k $= 1$, p $= 4$	3.378×10^{-09}	4.190×10^{-10}	1.126×10^{-09}	8.471
COT2, k $= 1$, p $= 4$	1.051×10^{-09}	1.303×10^{-10}	3.502×10^{-10}	8.979
COT3, k $= 1$, p $= 4$	1.003×10^{-09}	1.243×10^{-10}	3.342×10^{-10}	8.999
COT4, k $= 1$, p $= 4$	1.001×10^{-09}	1.241×10^{-10}	3.336×10^{-10}	9.000
NPOBM, k $= 1$, p $= 4$, [24]	7.576×10^{-08}	5.688×10^{-08}	5.394×10^{-08}	7.121

Table 2: The results for Problem 6.1 with N $= 2^7$ where x $\in [0, 10]$

Methods	Norm$_\infty$	RMSE	Mean	scd
COT1, k $= 1$, p $= 4$	2.208×10^{-10}	1.944×10^{-11}	7.361×10^{-11}	9.656
COT2, k $= 1$, p $= 4$	6.596×10^{-11}	5.807×10^{-12}	2.199×10^{-11}	10.181
COT3, k $= 1$, p $= 4$	6.264×10^{-11}	5.515×10^{-12}	2.088×10^{-11}	10.203
COT4, k $= 1$, p $= 4$	6.252×10^{-11}	5.505×10^{-12}	2.084×10^{-11}	10.204
NPOBM, k $= 1$, p $= 4$, [24]	1.016×10^{-09}	7.625×10^{-10}	7.230×10^{-10}	8.993

Table 3: The results for Problem 6.1 with N $= 2^8$ where x $\in [0, 10]$

Methods	Norm$_\infty$	RMSE	Mean	scd
COT1, k $= 1$, p $= 4$	1.412×10^{-11}	8.809×10^{-13}	4.707×10^{-12}	10.850
COT2, k $= 1$, p $= 4$	4.127×10^{-12}	2.575×10^{-13}	1.376×10^{-12}	11.384
COT3, k $= 1$, p $= 4$	3.909×10^{-12}	2.438×10^{-13}	1.303×10^{-12}	11.408
COT4, k $= 1$, p $= 4$	3.902×10^{-12}	2.434×10^{-13}	1.301×10^{-12}	11.409
NPOBM, k $= 1$, p $= 4$, [24]	1.461×10^{-11}	1.097×10^{-11}	1.040×10^{-11}	10.840

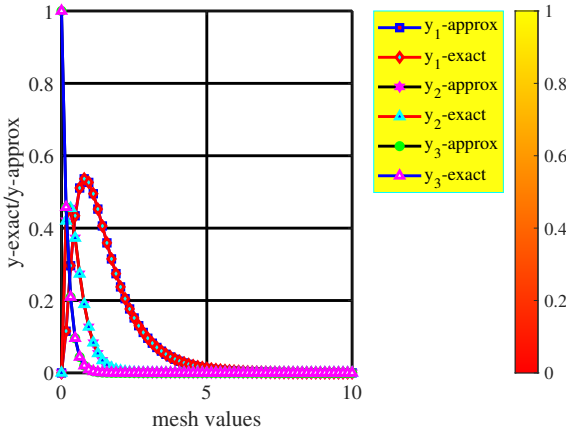

Figure 13: The accuracy curves of Problem 6.1 when NS $= 2^6$ for COT2

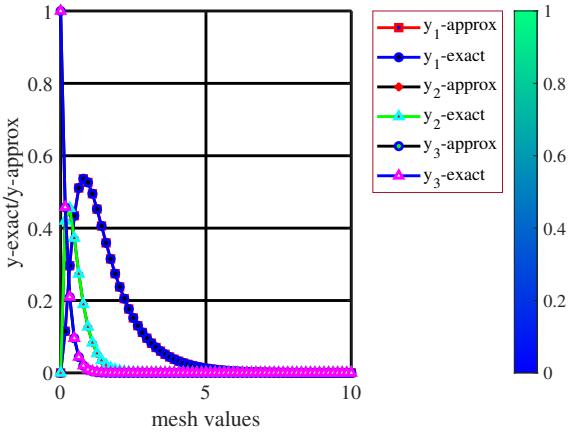

Figure 14: The accuracy curves of Problem 6.1 when NS $= 2^6$ for COT3

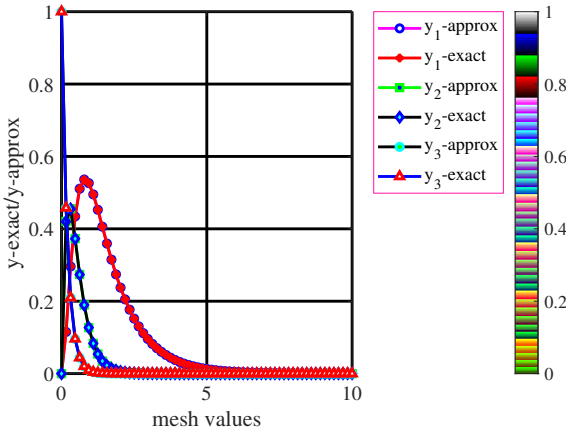

Figure 15: The accuracy curves of Problem 6.1 when NS $= 2^6$ for COT4

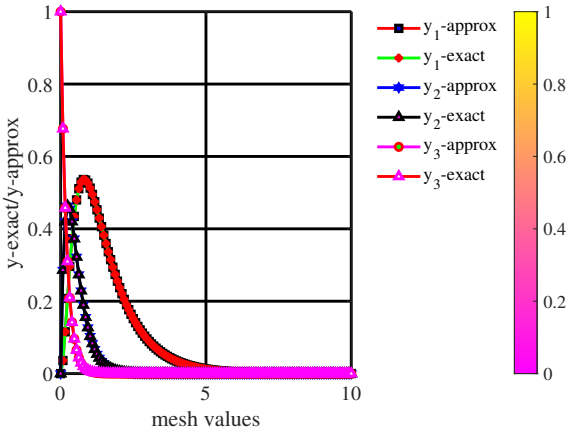

Figure 16: The accuracy curves of Problem 6.1 when NS $= 2^7$ for COT1

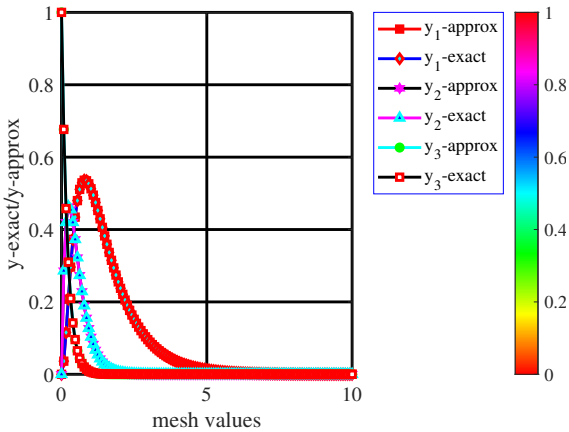

Figure 17: The accuracy curves of Problem 6.1 when NS $= 2^7$ for COT2

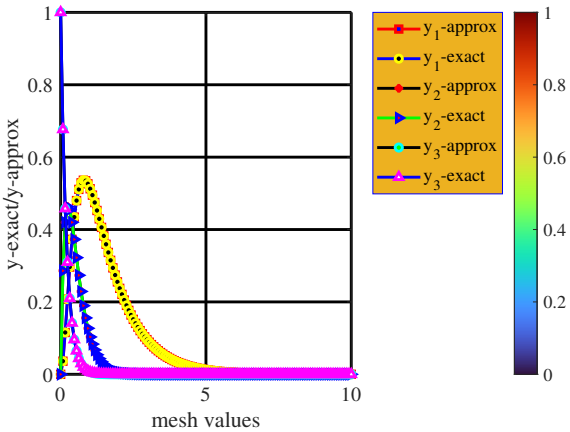

Figure 18: The accuracy curves of Problem 6.1 when NS $= 2^7$ for COT3

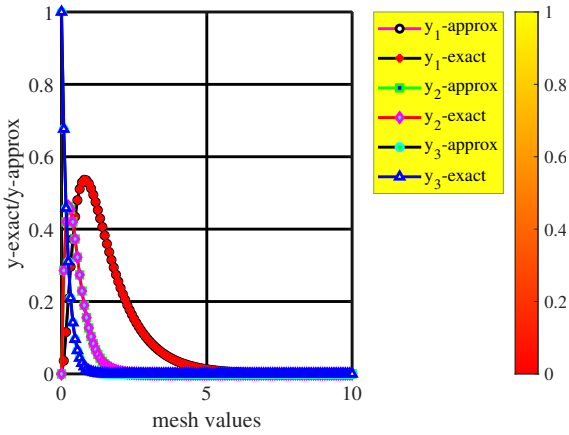

Figure 19: The accuracy curves of Problem 6.1 when NS $= 2^7$ for COT4

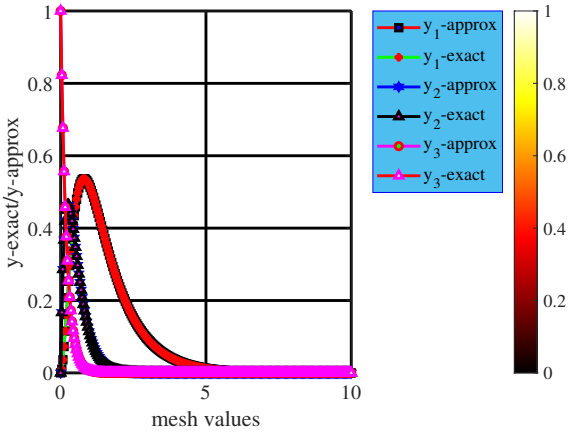

Figure 20: The accuracy curves of Problem 6.1 when NS $= 2^8$ for COT1

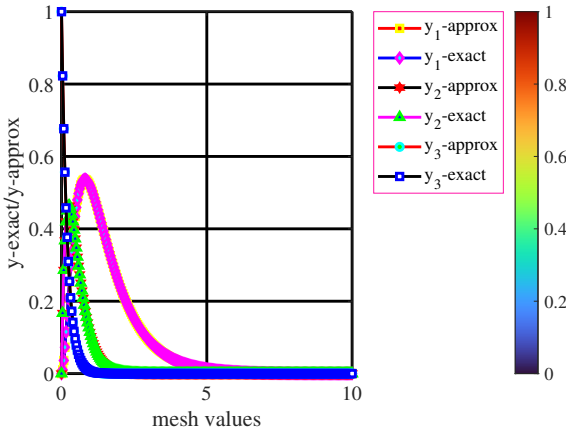

Figure 21: The accuracy curves of Problem 6.1 when NS $= 2^8$ for COT2

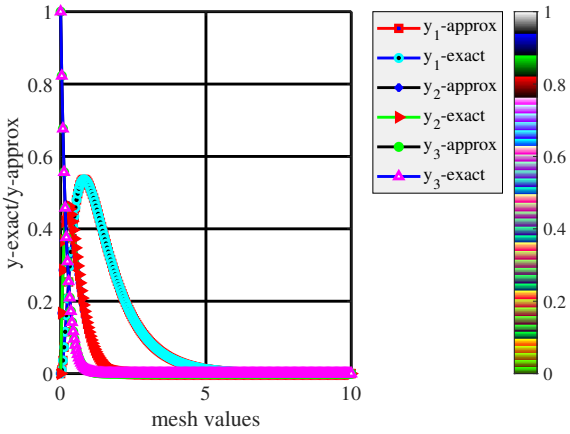

Figure 22: The accuracy curves of Problem 6.1 when NS $= 2^8$ for COT3

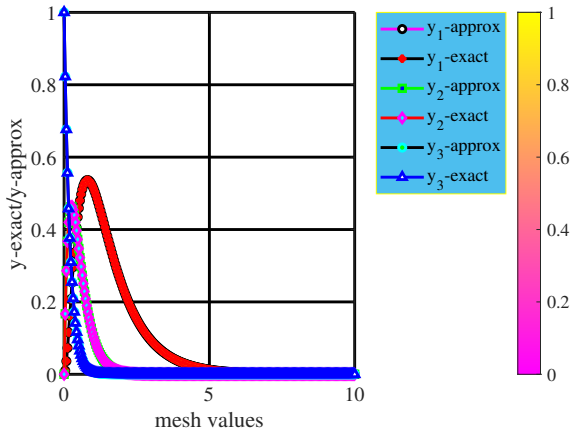

Figure 23: The accuracy curves of Problem 6.1 when NS $= 2^8$ for COT4

Problem 6.2. ***Nutrients flow in an aquarium as discussed by*** **Abuasbeh *et al.* [24]**

This flow is important for maintaining a healthy and balanced aquatic environment, as it supports the growth and survival of plants and animals in the aquarium. Imagine there is a body of water that has a radioactive isotope that is going to be utilized as a tracer for the food chain. The food chain is made up of several types of aquatic plankton, such as A and B. Plankton are defined as creatures that live in water and move with the low of the water, and may be found in such places as the Chesapeake Bay. There are two different kinds of plankton, which are known as phytoplankton and zooplankton. The phytoplankton are plant-like organisms that float across the water, including diatoms and other types of algae. Animal like organisms that float in the water known as zooplankton include copepods, larvae, and small crustaceans. More complex models might consider additional factors, such as the interactions between different types of plants and animals, the effects of different types of filtration systems, and the influence of water temperature and light intensity on the rate of photosynthesis. By considering these relationships, a differential equation model can provide a more comprehensive description of the nutrient flow in an aquarium and help to understand how changes in one aspect of the system might affect other parts of the system.The state variables $y_1(x), y_2(x), y_3(x)$ are explained as follows:
$y_1(x) =$ represents the concentration of an isotope in the water;
$y_2(x) =$ represents the concentration of an isotope in A; and
$y_3(x) =$ represents the concentration of an isotope in B.They are used in the following coupled linear system of differential equations

$$\begin{aligned}
y_1'(x) &= -3y_1(x) + 6y_2(x) + 5y_3(x), \qquad y_1(0) = 1,\\
y_2'(x) &= 2y_1(x) - 12y_2(x), \qquad y_2(0) = 0,\\
y_3'(x) &= y_1(x) + 6y_2(x) - 5y_3(x), \qquad y_3(0) = 0,
\end{aligned}$$

So that the exact solution is given by

$$\begin{aligned}
y_1(x) &= \frac{1}{282}(180 + e^{-10x}(102\cosh(\sqrt{6x}) + 29\sqrt{6x}\sinh(\sqrt{6x}))),\\
y_2(x) &= \frac{1}{141}(15 + e^{-10x}(-15\cosh(\sqrt{6x}) + 22\sqrt{6x}\sinh(\sqrt{6x}))),\\
y_3(x) &= \frac{1}{282}(72 + e^{-10x}(72\cosh(\sqrt{6x}) + 73\sqrt{6x}\sinh(\sqrt{6x}))).
\end{aligned}$$

The results from solving Problem 6.2 are presented in Tables 4–7 with its solution and accuracy curves Figure 26 and Figures 27–50. Figures 24 and 25 display well-defined surface plots for the dynamic differential systems and their exact functions, indicating an agreement and inter-relationship; and that for good initial guesses, non-divergent solutions are possible.
For Figure 26, it represents the solution curves from employing the lsode package that invokes the BDFs (Gear's method) to solve Problem 6.2. The choice of lsode MAPLE package evolve, since the need for a high accuracy and low tolerance are sufficient features. In Figures 27–38, they provide the accuracy plots in comparison of the approximate to analytical solutions. A quick look shows that approximate solutions are close to their true solutions. The results from Tables 4–7 clearly present improved accuracy in the suggested methods

in comparison to a class of optimal formulas with fixed and adaptive step size strategy proposed by Abuasbeh *et al.* [24]. Consequently, Table 7 and Figures 39–50 provide the table of results and their corresponding accuracy curves by setting different accuracy tolerance and total iteration numbers. From the table, we have that with decreased accuracy tolerance, improved accuracy is evident in the proposed methods.

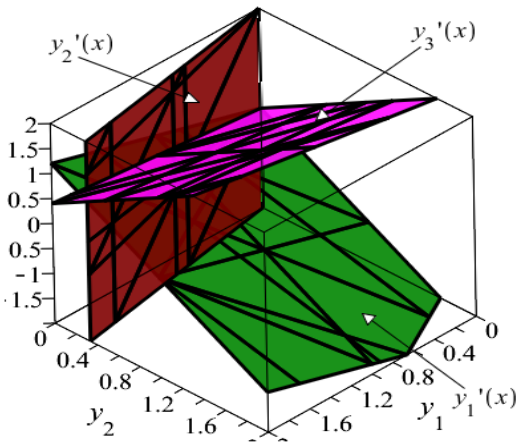

Figure 24: The function plots showing a physical interconnected surfaces of differential systems for Problem 6.2

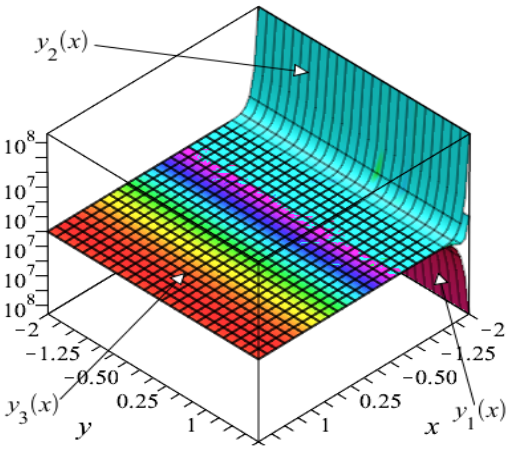

Figure 25: The exact function plots showing connected well-defined surfaces for Problem 6.2

Table 4: The results for Problem 6.2 with $N = 2^6$ where $x \in [0,5]$

Methods	$Norm_\infty$	RMSE	Mean	scd
COT1, $k=1, p=4$	4.163×10^{-16}	5.164×10^{-17}	1.388×10^{-16}	15.654
COT2, $k=1, p=4$	3.192×10^{-16}	3.959×10^{-17}	1.064×10^{-16}	15.654
COT3, $k=1, p=4$	1.804×10^{-16}	2.238×10^{-17}	6.014×10^{-17}	15.955
COT4, $k=1, p=4$	3.192×10^{-16}	3.959×10^{-17}	1.064×10^{-16}	15.654
NPOBM, $k=1, p=4$, [24]	7.337×10^{-09}	5.347×10^{-09}	4.891×10^{-09}	8.134

Table 5: The results for Problem 6.2 with $N = 2^7$ where $x \in [0,5]$

Methods	$Norm_\infty$	RMSE	Mean	scd
COT1, $k=1, p=4$	6.384×10^{-16}	5.621×10^{-17}	2.128×10^{-16}	15.353
COT2, $k=1, p=4$	9.576×10^{-16}	8.431×10^{-17}	3.192×10^{-16}	15.176
COT3, $k=1, p=4$	9.715×10^{-17}	8.553×10^{-18}	4.163×10^{-17}	15.955
COT4, $k=1, p=4$	2.637×10^{-16}	2.322×10^{-17}	8.789×10^{-17}	15.654
NPOBM, $k=1, p=4$, [24]	9.832×10^{-11}	7.167×10^{-11}	6.557×10^{-11}	10.01

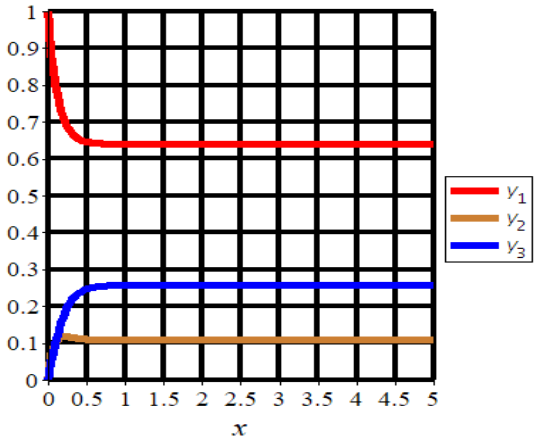

Figure 26: The MAPLE dsolve plot for Problem 6.2 when NS $= 2^6$

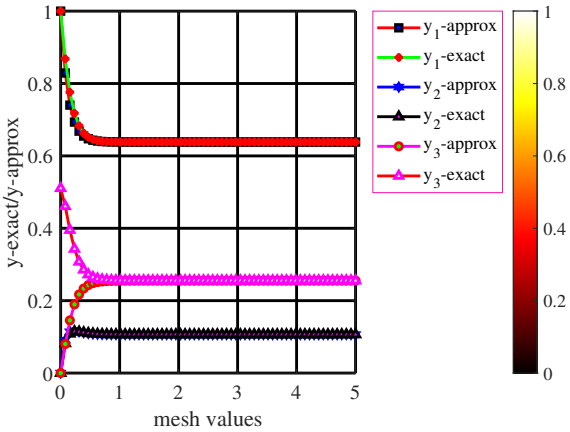

Figure 27: The accuracy curves of Problem 6.2 when NS $= 2^6$ for COT1

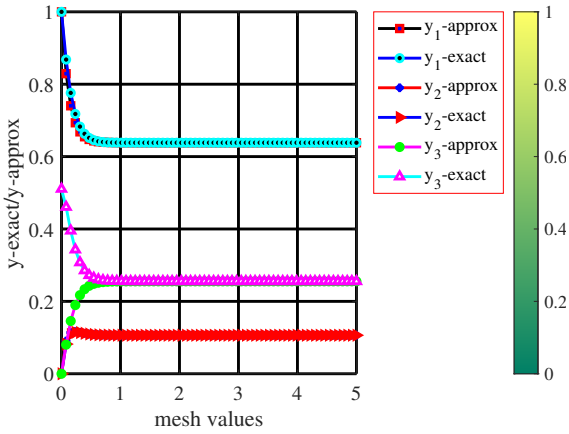

Figure 28: The accuracy curves of Problem 6.2 when NS $= 2^6$ for COT2

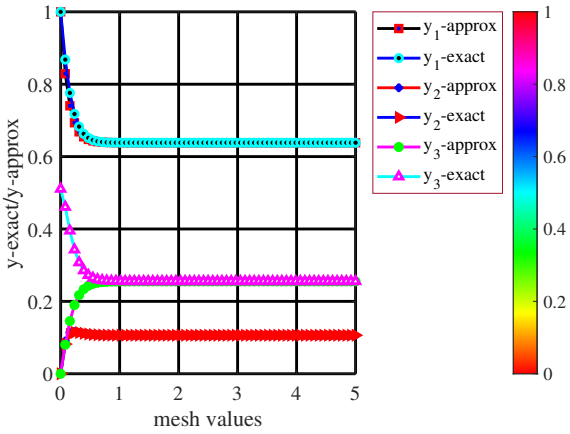

Figure 29: The accuracy curves of Problem 6.2 when NS $= 2^6$ for COT3

Table 6: The results for Problem 6.2 with N $= 2^8$ where x $\in [0, 5]$

Methods	**Norm$_\infty$**	**RMSE**	**Mean**	**scd**
COT1, k $= 1$, p $= 4$	3.608×10^{-16}	2.251×10^{-17}	1.573×10^{-16}	15.478
COT2, k $= 1$, p $= 4$	7.355×10^{-16}	4.588×10^{-17}	2.452×10^{-16}	15.256
COT3, k $= 1$, p $= 4$	6.800×10^{-16}	4.242×10^{-17}	2.267×10^{-16}	15.256
COT4, k $= 1$, p $= 4$	4.857×10^{-16}	3.030×10^{-17}	1.989×10^{-16}	15.353
NPOBM, k $= 1$, p $= 4$, [24]	1.416×10^{-12}	1.032×10^{-12}	9.449×10^{-13}	11.85

Table 7: The results for Problem 6.2 with varied iterations number with $x \in [0,5]$

tol	Methods	Norm_∞	RMSE	Mean	NS
	COT1, $k=1, p=4$	6.939×10^{-17}	1.792×10^{-17}	2.313×10^{-17}	14
10^{-3}	COT2, $k=1, p=4$	5.551×10^{-16}	1.433×10^{-16}	1.850×10^{-16}	14
	COT3, $k=1, p=4$	5.690×10^{-16}	1.469×10^{-16}	1.897×10^{-16}	14
	COT4, $k=1, p=4$	1.943×10^{-16}	5.017×10^{-17}	6.476×10^{-17}	14
	NPOBM, $k=1, p=4$, [24]	6.671×10^{-7}	8.005×10^{-7}	6.25×10^{-7}	14
	COT1, $k=1, p=4$	4.996×10^{-16}	9.277×10^{-17}	1.665×10^{-16}	28
10^{-4}	COT2, $k=1, p=4$	1.249×10^{-16}	2.319×10^{-17}	4.163×10^{-17}	28
	COT3, $k=1, p=4$	6.939×10^{-16}	1.289×10^{-16}	2.313×10^{-16}	28
	COT4, $k=1, p=4$	1.249×10^{-16}	2.319×10^{-17}	4.163×10^{-17}	28
	NPOBM, $k=1, p=4$, [24]	1.368×10^{-08}	1.368×10^{-08}	1.087×10^{-08}	28
	COT1, $k=1, p=4$	1.804×10^{-16}	2.349×10^{-17}	6.014×10^{-17}	58
10^{-5}	COT2, $k=1, p=4$	1.943×10^{-16}	2.529×10^{-17}	6.476×10^{-17}	58
	COT3, $k=1, p=4$	1.943×10^{-16}	2.529×10^{-17}	6.476×10^{-17}	58
	COT4, $k=1, p=4$	1.804×10^{-16}	2.349×10^{-17}	6.014×10^{-17}	58
	NPOBM, $k=1, p=4$, [24]	2.702×10^{-10}	2.702×10^{-10}	2.069×10^{-10}	58

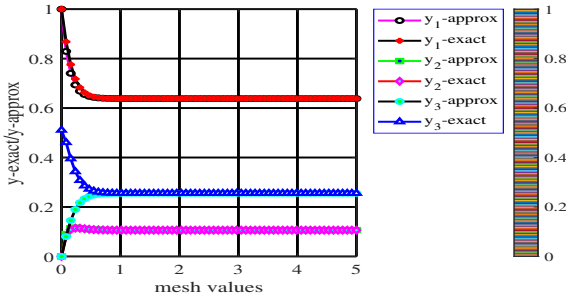

Figure 30: The accuracy curves of Problem 6.2 when $NS = 2^6$ for COT4

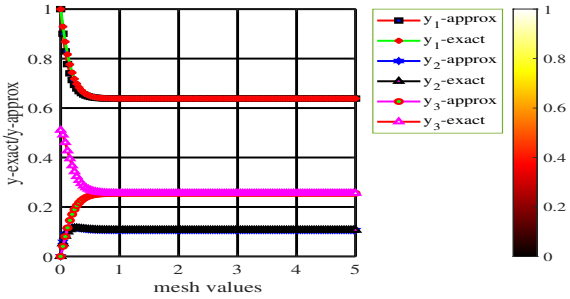

Figure 31: The accuracy curves of Problem 6.2 when $NS = 2^7$ for COT1

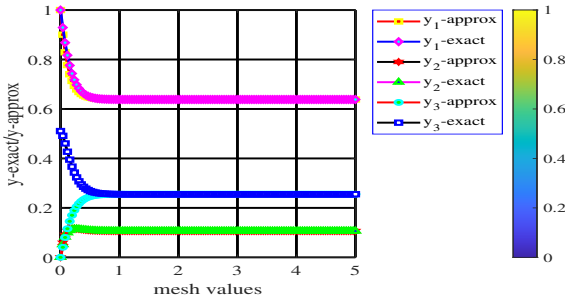

Figure 32: The accuracy curves of Problem 6.2 when $NS = 2^7$ for COT2

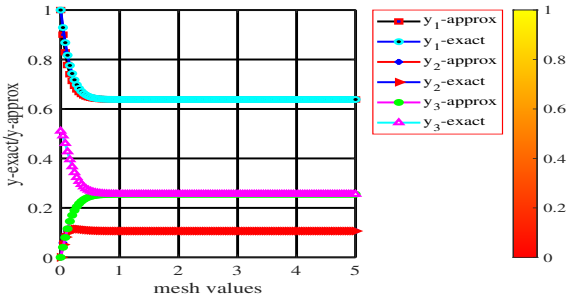

Figure 33: The accuracy curves of Problem 6.2 when $NS = 2^7$ for COT3

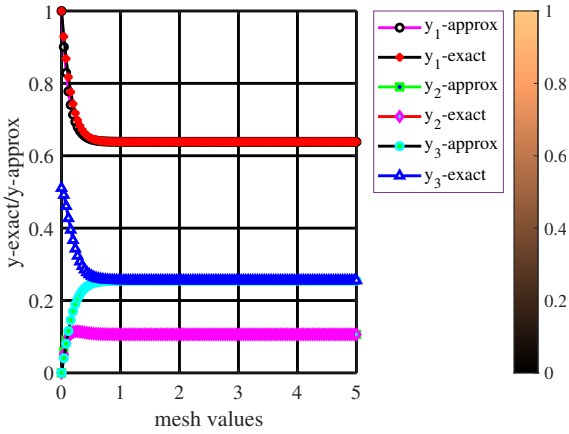

Figure 34: The accuracy curves of Problem 6.2 when NS $= 2^7$ for COT4

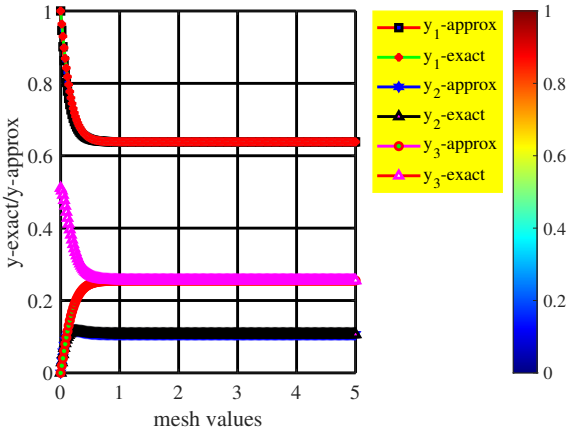

Figure 35: The accuracy curves of Problem 6.2 when NS $= 2^8$ for COT1

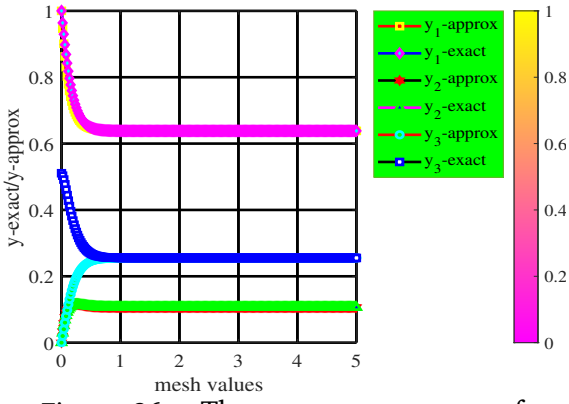

Figure 36: The accuracy curves of Problem 6.2 when NS $= 2^8$ for COT2

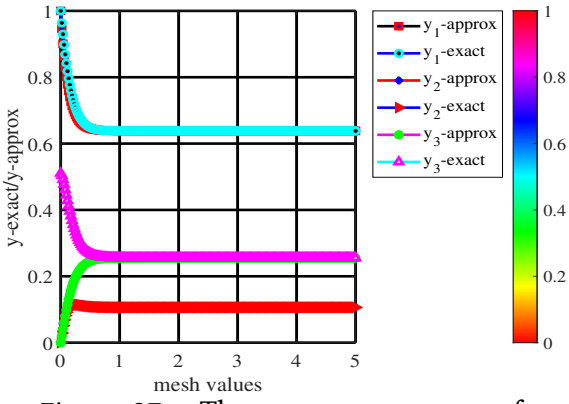

Figure 37: The accuracy curves of Problem 6.2 when NS $= 2^8$ for COT3

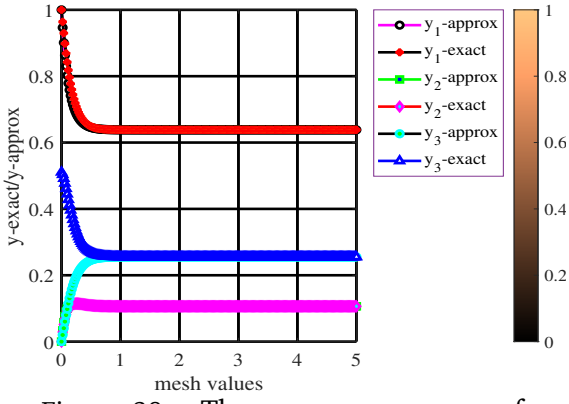

Figure 38: The accuracy curves of Problem 6.2 when NS $= 2^8$ for COT4

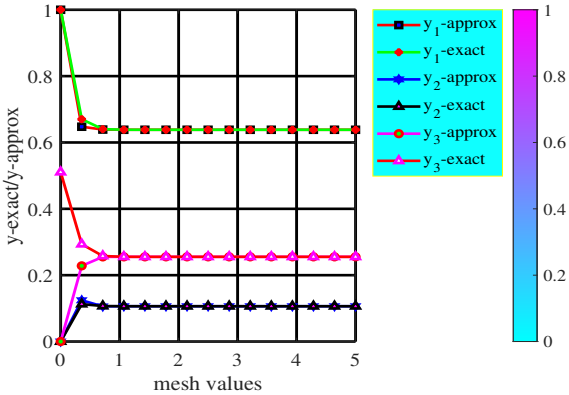

Figure 39: The accuracy curves of Problem 6.2 when NS $= 14$ and tol$= 10^{-3}$ for COT1

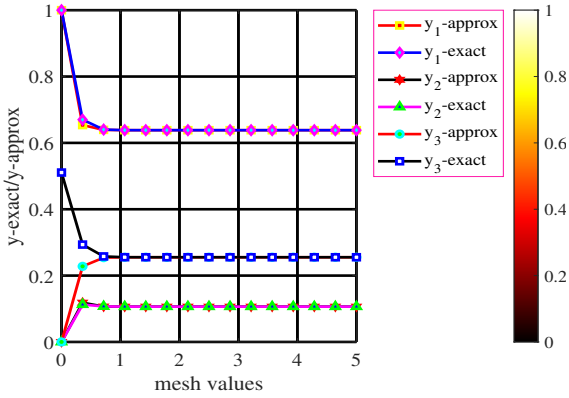

Figure 40: The accuracy curves of Problem 6.2 when NS = 14 and tol= 10^{-3} for COT2

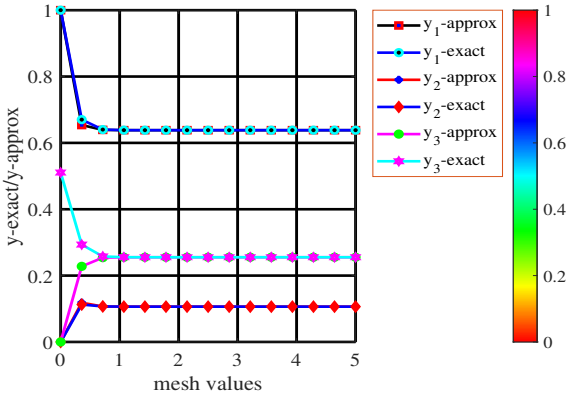

Figure 41: The accuracy curves of Problem 6.2 when NS = 14 and tol= 10^{-3} for COT3

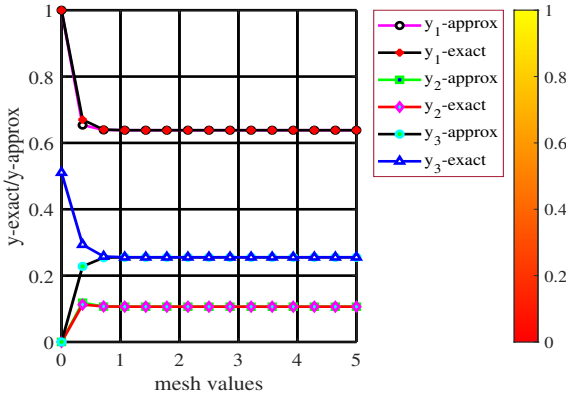

Figure 42: The accuracy curves of Problem 6.2 when NS = 14 and tol= 10^{-3} for COT4

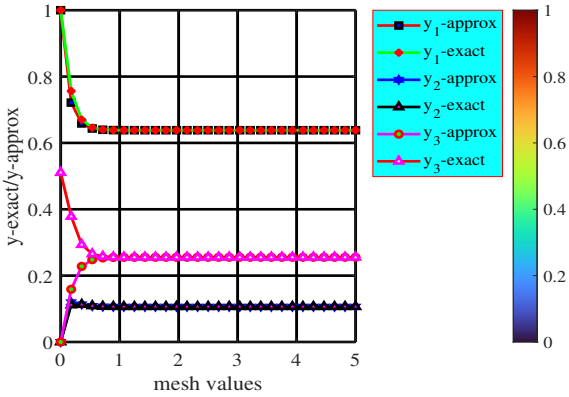

Figure 43: The accuracy curves of Problem 6.2 when NS = 28 and tol= 10^{-4} for COT1

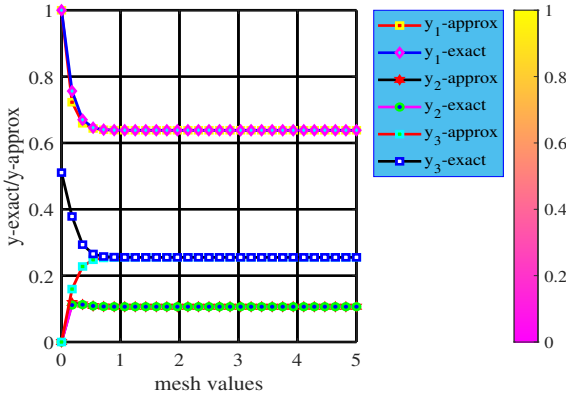

Figure 44: The accuracy curves of Problem 6.2 when NS = 28 and tol= 10^{-4} for COT2

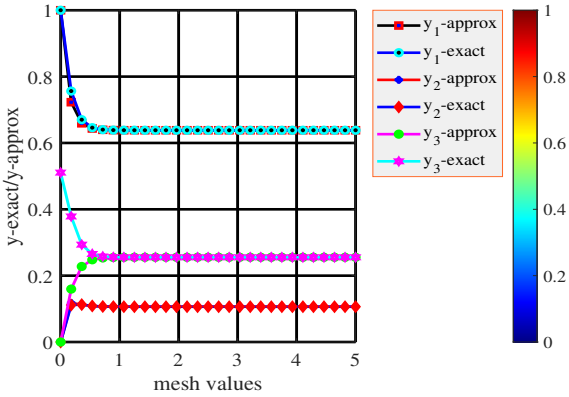

Figure 45: The accuracy curves of Problem 6.2 when NS = 28 and tol= 10^{-4} for COT3

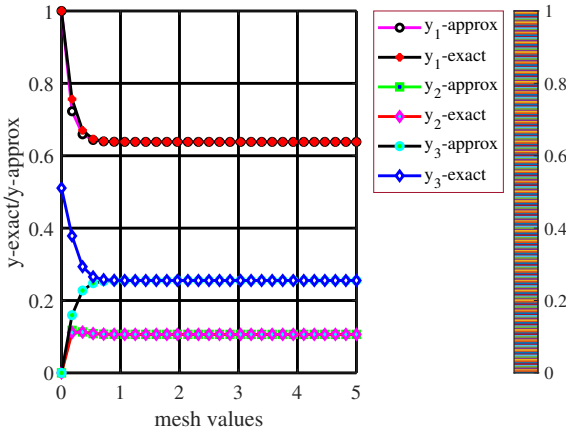

Figure 46: The accuracy curves of Problem 6.2 when NS = 28 and tol= 10^{-4} for COT4

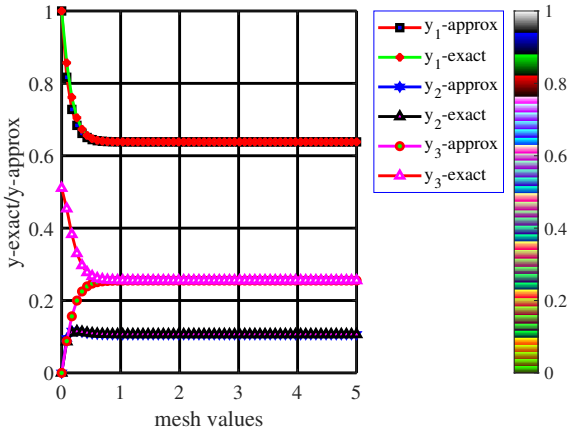

Figure 47: The accuracy curves of Problem 6.2 when NS = 58 and tol= 10^{-5} for COT1

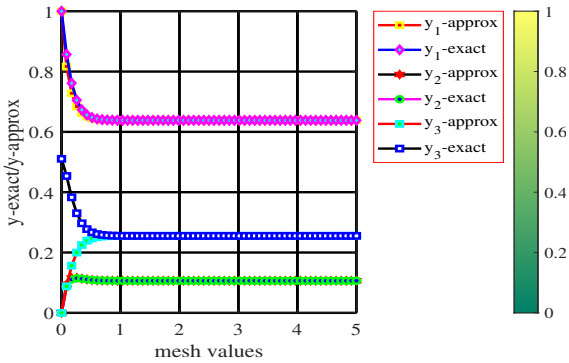

Figure 48: The accuracy curves of Problem 6.2 when NS = 58 and tol= 10^{-5} for COT2

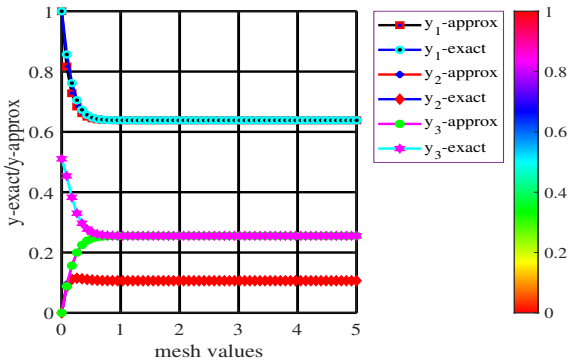

Figure 49: The accuracy curves of Problem 6.2 when NS = 58 and tol= 10^{-5} for COT3

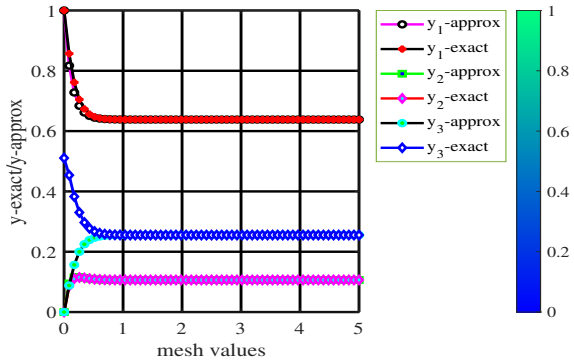

Figure 50: The accuracy curves of Problem 6.2 when NS = 58 and tol= 10^{-5} for COT4

Problem 6.3. ***The resonance vibration in a machine in mechanical engineering as considered by*** **Abuasbeh *et al.* [25]**

A practical problem on resonance vibration of a machine was modeled as

$$2000y''(x) + (2 \times 10^5)y(x) = 2000\sin(10x), \qquad y(0) = 0.1, \qquad y'(0) = 0, \qquad h = 0.01,$$

whose analytical solution is given by:

$$y(x) = \frac{1}{10}\cos(10x) + \frac{1}{200}\sin(10x) - \frac{x}{20}\cos(10x).$$

The results from simulating Problem 6.3 are shown in Table 8. In Figure 51, a well-defined differential surface plots showing connected systems is given. Figure 52 is a special exact surface plots showing oscillatory behavior. This physical characterisitic is clearly evident in the results from Table 8. For Figures 53–55, they depict the solution curves using lsode MAPLE dsolve package and the new formulas, showing close approximations with the analytical solutions.

Problem 6.3 is another special application problem in mechanical engineering, the resonance vibration in a machine. It is modeled into a second-order differential system. With the results displayed in Table 8, it is clear that COT1 and COT2 provide appreciable level of accuracy, though without convergence. However, COT2 presents better accuracy over COT1, indicating that the proposed techniques could yield better accuracy and probably convergence, if different mesh sizes are considered.

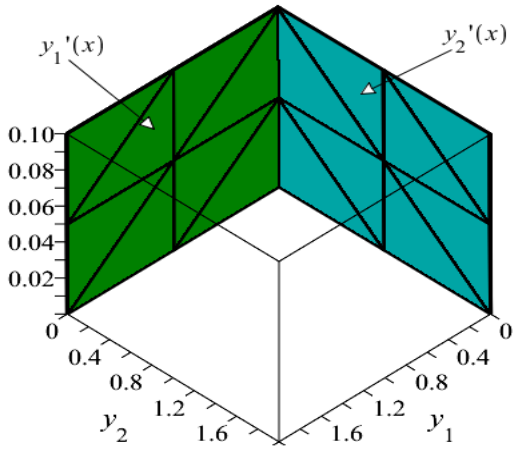

Figure 51: The function plots showing well-defined connected surface plots for Problem 6.3

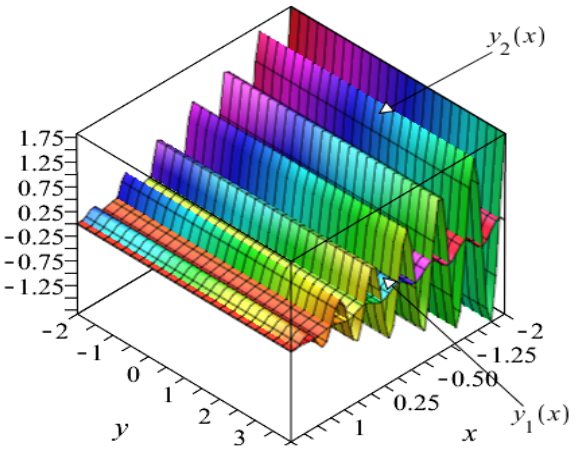

Figure 52: The exact function plots showing a physical relation of connected systems for Problem 6.3

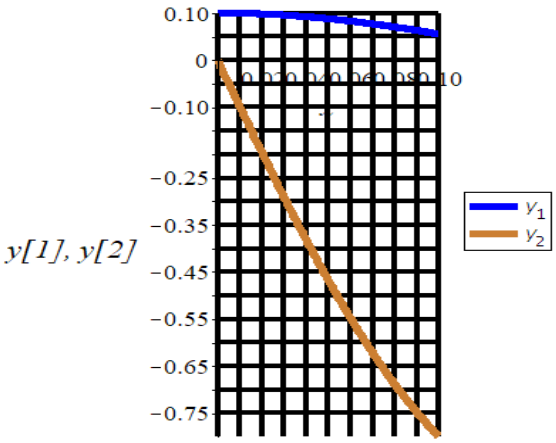

Figure 53: The MAPLE dsolve plot for Problem 6.3 when $h = 0.01$

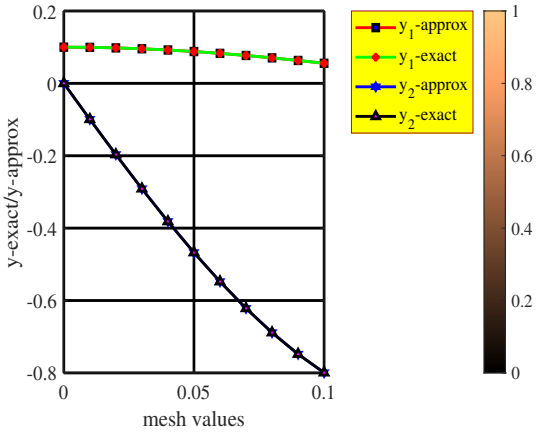

Figure 54: The accuracy curves of Problem 6.3 when $h = 0.01$ and $x \in [0, 0.10]$ for COT1

Table 8: The absolute error for Problem 6.3 with $x \in [0, 0.10]$

x	EIOBSOH, [25]		COT1,	COT2,
	$k = 1, p = 4$	y_i	$k = 1, p = 4$	$k = 1, p = 4$
0.01	3.24740×10^{-15}	y_1	2.21823×10^{-13}	6.21864×10^{-14}
		y_2	7.05741×10^{-12}	2.02081×10^{-12}
0.02	5.66951×10^{-12}	y_1	5.81660×10^{-13}	1.63911×10^{-13}
		y_2	1.35293×10^{-11}	3.87671×10^{-12}
0.03	1.67078×10^{-11}	y_1	1.06927×10^{-12}	3.02286×10^{-13}
		y_2	1.92152×10^{-11}	5.51020×10^{-12}
0.04	3.27208×10^{-11}	y_1	1.67195×10^{-12}	4.73704×10^{-13}
		y_2	2.39303×10^{-11}	6.86806×10^{-12}
0.05	5.32108×10^{-11}	y_1	2.37460×10^{-12}	6.73892×10^{-13}
		y_2	2.75087×10^{-11}	7.90290×10^{-12}
0.06	7.75898×10^{-11}	y_1	3.16006×10^{-12}	8.97948×10^{-13}
		y_2	2.98062×10^{-11}	8.57314×10^{-12}
0.07	1.05189×10^{-10}	y_1	4.00928×10^{-12}	1.14045×10^{-12}
		y_2	3.07023×10^{-11}	8.84393×10^{-12}
0.08	1.35271×10^{-10}	y_1	4.90175×10^{-12}	1.39556×10^{-12}
		y_2	3.01039×10^{-11}	8.68850×10^{-12}
0.09	1.67042×10^{-10}	y_1	5.81572×10^{-12}	1.65711×10^{-12}
		y_2	2.79445×10^{-11}	8.08742×10^{-12}
0.10	1.99664×10^{-10}	y_1	6.72872×10^{-12}	1.91865×10^{-12}
		y_2	2.41873×10^{-11}	7.02971×10^{-12}

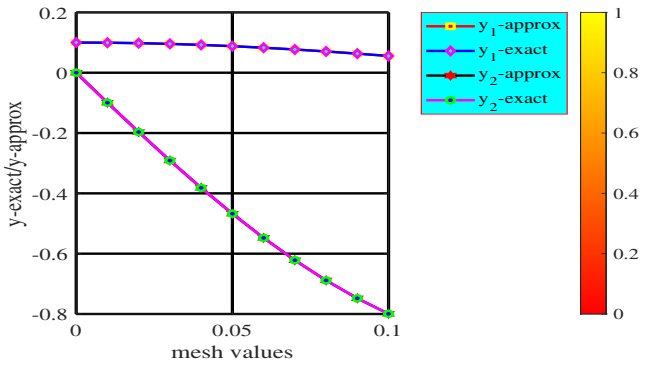

Figure 55: The accuracy curves of Problem 6.3 when $h = 0.01$ and $x \in [0, 0.10]$ for COT2

Problem 6.4. ***Consider the two-dimensional nonlinear system of ODEs taken from*** **Abuasbeh *et al.* [24]**

$$y_1'(x) = \mu y_1(x) + y_2^2(x), \qquad y_1(0) = \frac{-1}{\mu+2}, \qquad x \in [0, 20],$$
$$y_2'(x) = -y_2(x), \qquad y_2(0) = 1, \qquad \mu = -10^3,$$

the exact solution is taken to be

$$y_1(x) = \frac{-e^{-2x}}{\mu+2},$$
$$y_2(x) = e^{-x}.$$

The numerical results from solving Problem 6.4 are provided in Tables 9–11 over the integration interval $[0, 20]$. A well-defined three-dimensional surface plots are given in Figures 56 and 57, indicating connected differential systems and a physical relation between exact functions. The efficiency plots are shown in Figures 59–70. Figure 58 represent the phaseportraits plots. It provides the trajectories with the red marker indicating point of convergence of the flow lines at the origin. Therefore, for Problem 6.4, a two-dimensional non-linear system, is further solved using the intended formulas. The new methods are applied over the integration interval $[0, 20]$. Tables 9–11 present the results while Figures 59–70 give the efficiency curves. From the foregoing tables, it is clear that the proposed formulas performed excellently while COT4 performs better in the overall varied step-number with high precision factor. The accuracy curves show improved results as iterations proceed over the integration interval.

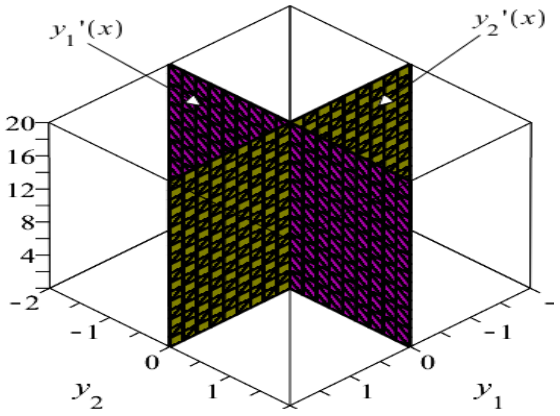

Figure 56: The function plots showing a connected well-defined surfaces for Problem 6.4

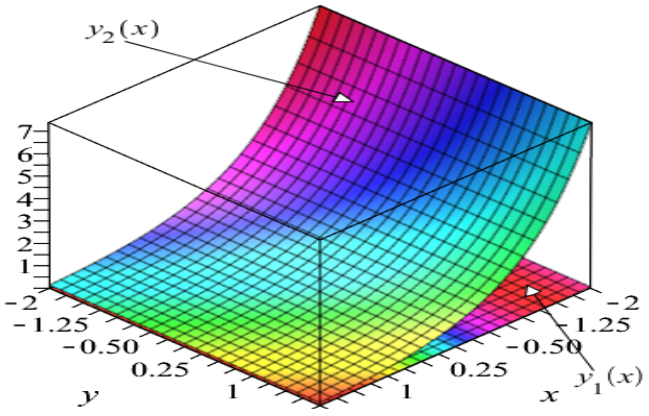

Figure 57: The exact function plots showing physically connected systems in Problem 6.4

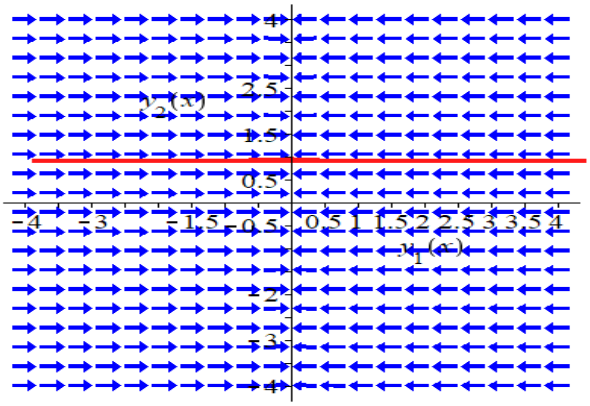

Figure 58: The phase portrait plots showing flow lines, whose tangent vectors and velocity are everywhere parallel except at $(x_0, y_0) = (0,0)$ for Problem 6.4

Table 9: The results for Problem 6.4 with NS=2^6 where $x \in [0,20]$

Methods	**Norm$_\infty$**	**RMSE**	**Mean**	**scd**
COT1, $k=1, p=4$	2.399×10^{-12}	2.976×10^{-13}	1.200×10^{-12}	11.620
COT2, $k=1, p=4$	8.013×10^{-13}	9.939×10^{-14}	4.007×10^{-13}	12.096
COT3, $k=1, p=4$	7.705×10^{-13}	9.557×10^{-14}	3.853×10^{-13}	12.113
COT4, $k=1, p=4$	7.695×10^{-13}	9.544×10^{-14}	3.847×10^{-13}	12.114
NPOBM, $k=1, p=4$ [24]	7.816×10^{-09}	5.527×10^{-09}	3.917×10^{-09}	8.107

Table 10: The results for Problem 6.4 with NS=2^7 where $x \in [0,20]$

Methods	$Norm_\infty$	RMSE	Mean	scd
COT1, $k=1,p=4$	1.636×10^{-13}	1.440×10^{-14}	8.179×10^{-14}	12.786
COT2, $k=1,p=4$	5.088×10^{-14}	4.480×10^{-15}	2.544×10^{-14}	13.294
COT3, $k=1,p=4$	4.855×10^{-14}	4.274×10^{-15}	2.427×10^{-14}	13.314
COT4, $k=1,p=4$	4.847×10^{-14}	4.267×10^{-15}	2.423×10^{-14}	13.315
NPOBM, $k=1,p=4$, [24]	1.070×10^{-10}	7.573×10^{-11}	5.530×10^{-11}	9.970

Table 11: The results for Problem 6.4 with NS=2^8 where $x \in [0,20]$

Methods	$Norm_\infty$	RMSE	Mean	scd
COT1, $k=1,p=4$	1.069×10^{-14}	6.671×10^{-16}	5.347×10^{-15}	13.971
COT2, $k=1,p=4$	3.194×10^{-15}	1.993×10^{-16}	1.597×10^{-15}	14.496
COT3, $k=1,p=4$	3.033×10^{-15}	1.892×10^{-16}	1.5166×10^{-15}	14.518
COT4, $k=1,p=4$	3.028×10^{-15}	1.889×10^{-16}	1.5139×10^{-15}	14.519
NPOBM, $k=1,p=4$, [24]	1.571×10^{-12}	1.229×10^{-12}	1.156×10^{-12}	11.80

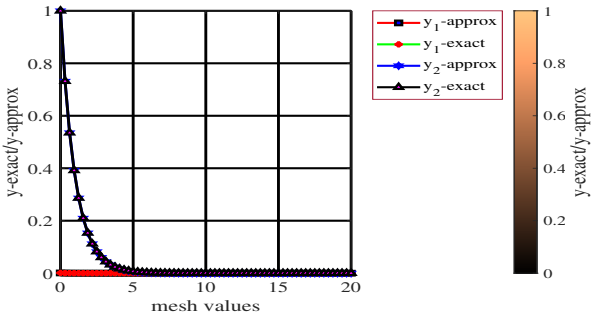

Figure 59: The accuracy curves of Problem 6.4 when NS = 2^6 and $x \in [0,20]$ for COT1

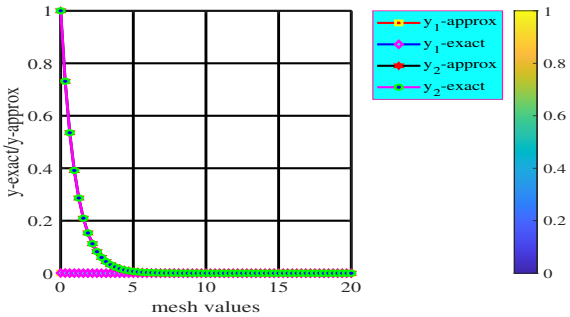

Figure 60: The accuracy curves of Problem 6.4 when NS = 2^6 and $x \in [0,20]$ for COT2

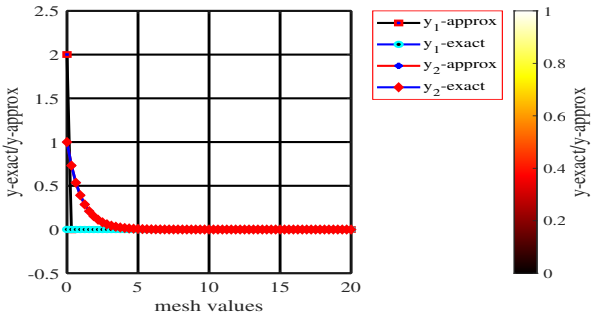

Figure 61: The accuracy curves of Problem 6.4 when NS = 2^6 and $x \in [0,20]$ for COT3

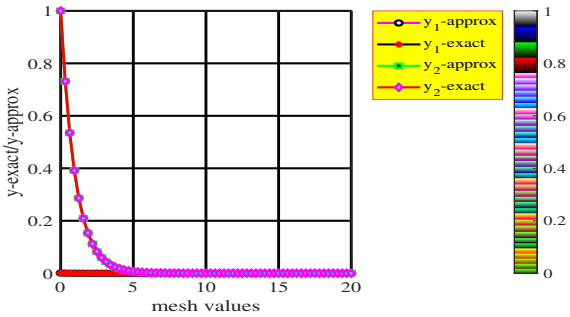

Figure 62: The accuracy curves of Problem 6.4 when NS = 2^6 and $x \in [0,20]$ for COT4

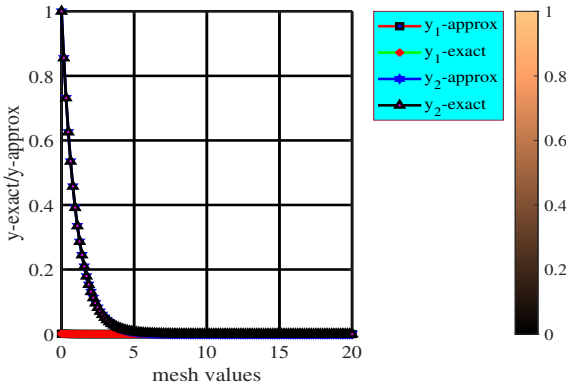

Figure 63: The accuracy curves of Problem 6.4 when NS $= 2^7$ and x $\in$ [0, 20] for COT1

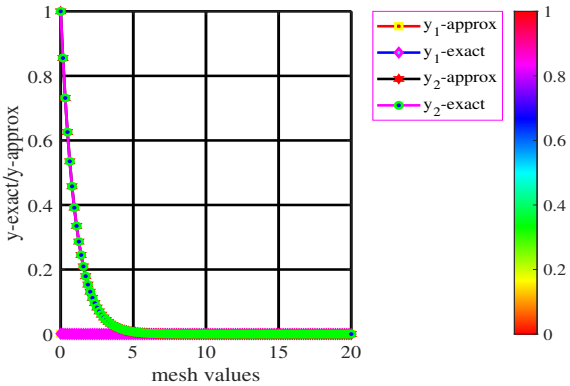

Figure 64: The accuracy curves of Problem 6.4 when NS $= 2^7$ and x $\in$ [0, 20] for COT2

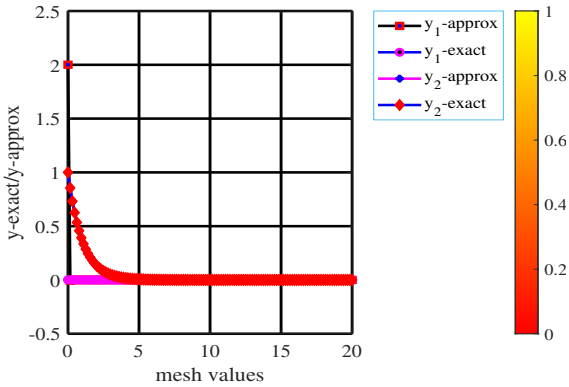

Figure 65: The accuracy curves of Problem 6.4 when NS $= 2^7$ and x $\in$ [0, 20] for COT3

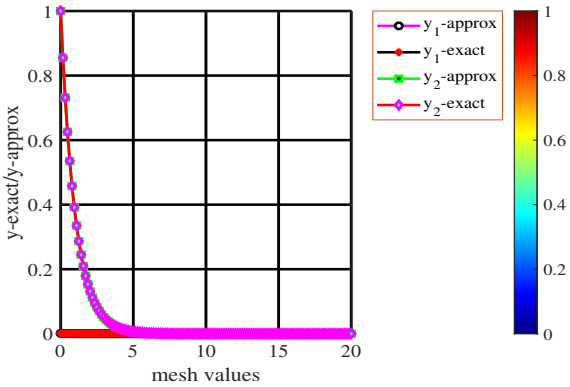

Figure 66: The accuracy curves of Problem 6.4 when NS $= 2^7$ and x $\in$ [0, 20] for COT4

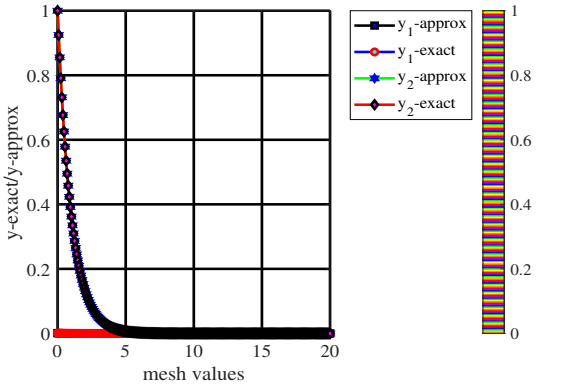

Figure 67: The accuracy curves of Problem 6.4 when NS $= 2^8$ and x $\in$ [0, 20] for COT1

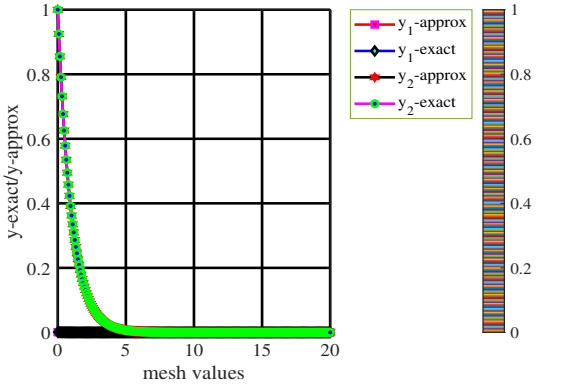

Figure 68: The accuracy curves of Problem 6.4 when NS $= 2^8$ and x $\in$ [0, 20] for COT2

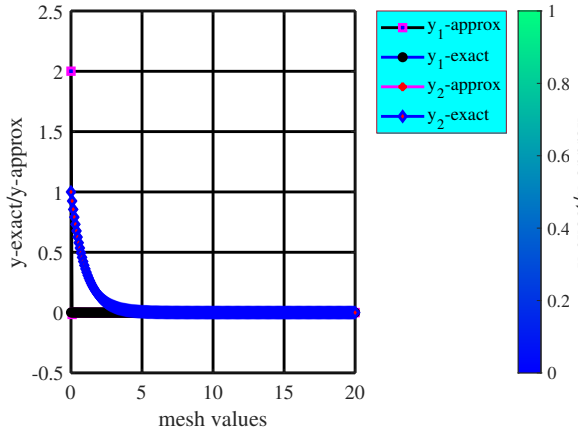

Figure 69: The accuracy curves of Problem 6.4 when NS $= 2^8$ and $x \in [0, 20]$ for COT3

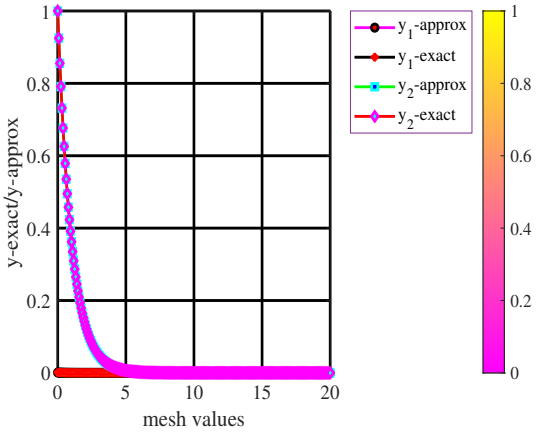

Figure 70: The accuracy curves of Problem 6.4 when NS $= 2^8$ and $x \in [0, 20]$ for COT4

Problem 6.5. ***Consider the two-dimensional nonlinear system taken from*** **Akinola *et al.* [23]**

$$\begin{bmatrix} y_1(x) \\ y_2(x) \end{bmatrix} = \begin{bmatrix} -1002y_1(x) - 1000y_2^2(x) \\ y_1(x) - y_2(x) - y_2^2(x) \end{bmatrix}, \qquad y_1(0) = 1, \qquad y_2(0) = 1, \qquad h = 0.1,$$

with the exact solution as

$$\begin{bmatrix} y_1(x) \\ y_2(x) \end{bmatrix} = \begin{bmatrix} e^{-2x} \\ e^{-x} \end{bmatrix}.$$

The simulation of Problem 6.5, its results and accuracy curves are as shown in Table 12 and Figures 74–82. The exact function and differential plots is shown in Figures 71 and 72, indicating connected systems. The phaseportraits in Figure 73 shows trajectories, in which the arrows converge at the origin for both components axes, where the tangent and velocity are everywhere parallel. The marker indicates the point and direction from which the flow lines are traced. In Figure 74, we see solution curves from employing the lsode MAPLE package that invokes the BDFs, which totally agreed with the accuracy curves for the proposed techniques. This compared method uses a minimal accuracy tolerance of 1×10^{-7}. Additionally, Problem 6.5 is a special non-linear problem whose eigenvalues are close to the imaginary axes. Usually, this type of problem is hard to solve if small step numbers are considered. It has eigenvalues $\lambda_1 = -1001$ and $\lambda_2 = -1$. The results are displayed in Table 12 at varied mesh sizes $[0, 5]$,$[0,100]$ and $[0, 250]$ with CPU time (seconds) using $h = 0.1$. It is evident for all derived formulas that when the mesh-size is set at $[0, 50]$, the methods showed improved accuracy with COT4 leading in accuracy while comparison with an order 9 method proposed by Akinola *et al.* [23], shows that the suggested formulas presented improved accuracy with increased mesh sizes. While the accuracy curves in Figures 75–82 depict close solutions, the CPU time (seconds) in Table 12, clearly presents better efficiency over the integration intervals.

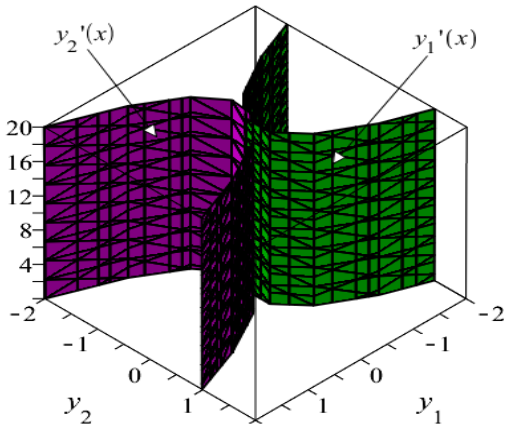

Figure 71: The function plots showing connected well-defined surfaces for Problem 6.5

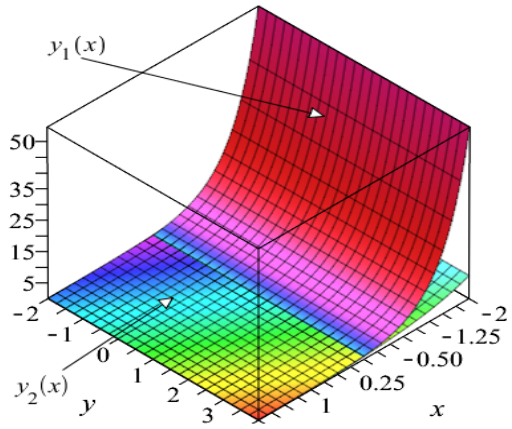

Figure 72: The exact function plot for Problem 6.5

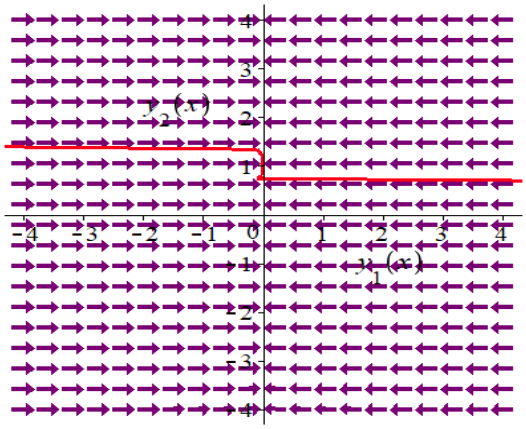

Figure 73: The phaseportrait function plot for Problem 6.5

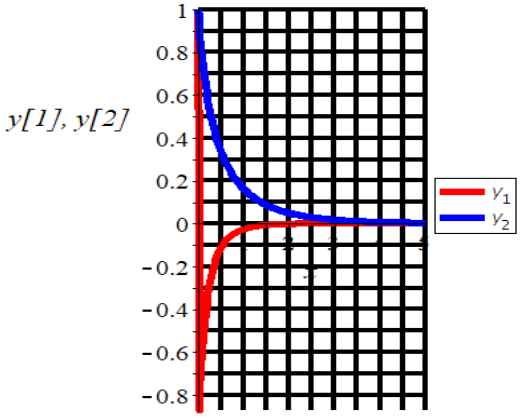

Figure 74: The solution plots using the embedded lsode MAPLE package for Problem 6.5

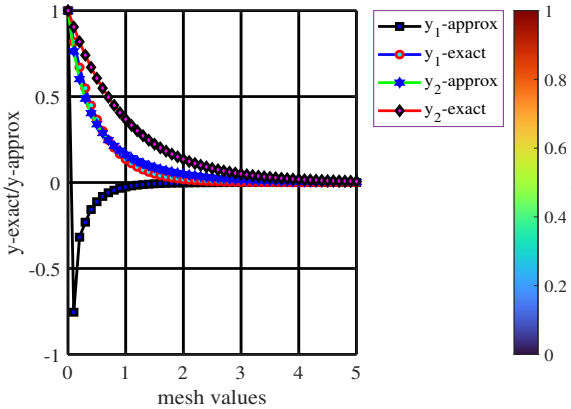

Figure 75: The accuracy curves of Problem 6.5 when $x \in [0,5]$ for COT1

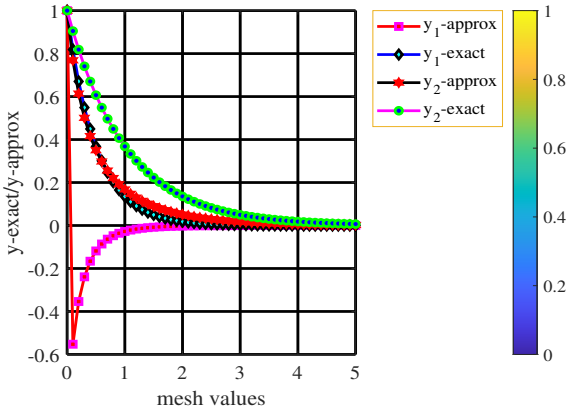

Figure 76: The accuracy curves of Problem 6.5 when $x \in [0,5]$ for COT2

Table 12: The absolute error for Problem 6.5 with varied mesh values, where $h = 0.1$

Methods	**Mesh sizes** (x)	y_i	**Error**	**CPU Time**
COT1, $k = 1, p = 4$	5	y_1	$5.04098267400969\times10^{-05}$	
		y_2	$4.48898885957800\times10^{-03}$	0.0540
	50	y_1	$4.12691683227591\times10^{-44}$	
		y_2	$1.287892898629811\times10^{-22}$	0.0579
	100	y_1	$1.53523400968903\times10^{-87}$	
		y_2	$2.48406572827684\times10^{-44}$	0.3209
	250	y_1	$7.90353136661776\times10^{-218}$	
		y_2	$1.78243246765622\times10^{-109}$	0.3346
COT2, $k = 1, p = 4$	5	y_1	$5.074712714667810\times10^{-05}$	
		y_2	$4.41262937774854\times10^{-03}$	0.0397
	50	y_1	$4.15428364098105\times10^{-44}$	
		y_2	$1.26615889292969\times10^{-22}$	0.0876
	100	y_1	$1.54542172065870\times10^{-87}$	
		y_2	$2.44211704971267\times10^{-44}$	0.3305
	250	y_1	$7.95608861021622\times10^{-218}$	
		y_2	$1.75227100049523\times10^{-109}$	0.3451
COT3, $k = 1, p = 4$	5	y_1	$5.074742339959760\times10^{-05}$	
		y_2	$4.41256027608344\times10^{-03}$	0.0678
	50	y_1	$4.15430807835389\times10^{-44}$	
		y_2	$1.26613892636515\times10^{-22}$	0.0808
	100	y_1	$1.54543097595476\times10^{-87}$	
		y_2	$2.44207788849194\times10^{-44}$	0.2035
	250	y_1	$7.95613879733890\times10^{-218}$	
		y_2	$1.75224150132313\times10^{-109}$	0.3477
COT4, $k = 1, p = 4$	5	y_1	$5.07509219036483\times10^{-05}$	
		y_2	$4.41180422451567\times10^{-03}$	0.0561
	50	y_1	$4.15459174220851\times10^{-44}$	
		y_2	$1.26592380571122\times10^{-22}$	0.0670
	100	y_1	$1.54553650452454\times10^{-87}$	
		y_2	$2.44166295673159\times10^{-44}$	0.1993
	250	y_1	$7.95668213298876\times10^{-218}$	
		y_2	$1.75194374542110\times10^{-109}$	0.3277
Method in [23], $k = 4, p = 11$	5	y_1	$2.64615455331249\times10^{-05}$	
		y_2	$1.78144787057234\times10^{-03}$	0.2173
	50	y_1	$3.97220625567371\times10^{-41}$	
		y_2	$1.81946223485350\times10^{-21}$	1.8539

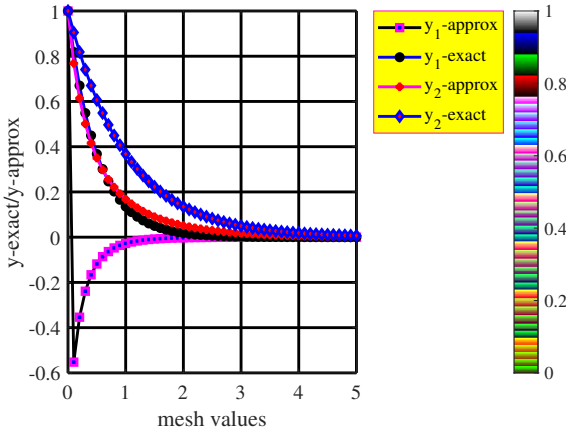

Figure 77: The accuracy curves of Problem 6.5 when $x \in [0,5]$ for COT3

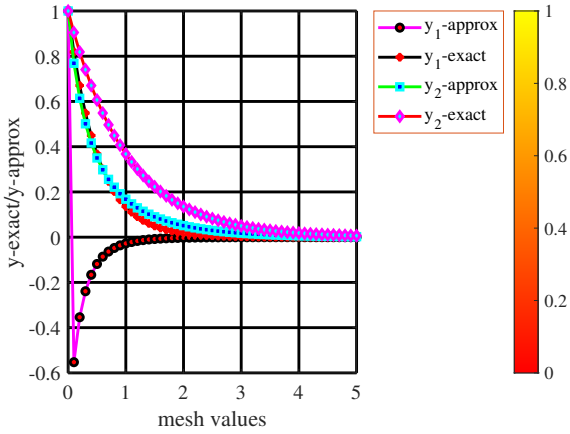

Figure 78: The accuracy curves of Problem 6.5 when $x \in [0,5]$ for COT4

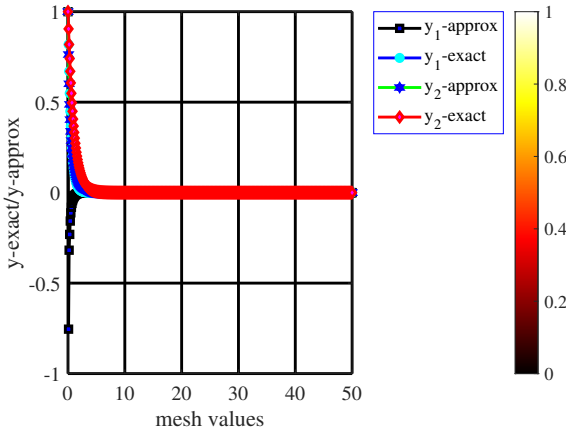

Figure 79: The accuracy curves of Problem 6.5 when $x \in [0,50]$ for COT1

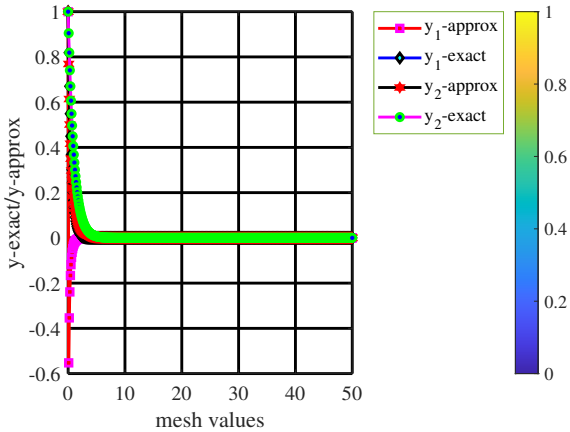

Figure 80: The accuracy curves of Problem 6.5 when $x \in [0,50]$ for COT2

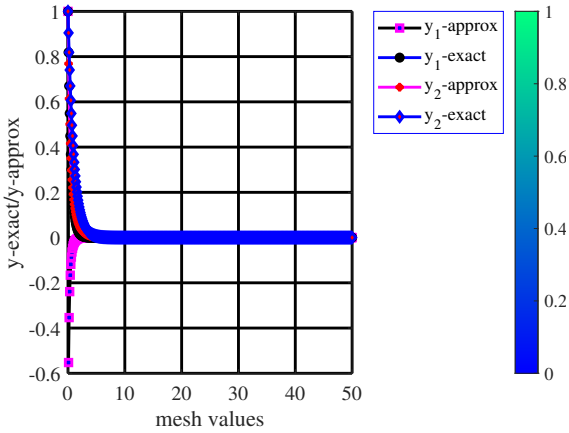

Figure 81: The accuracy curves of Problem 6.5 when $x \in [0,50]$ for COT3

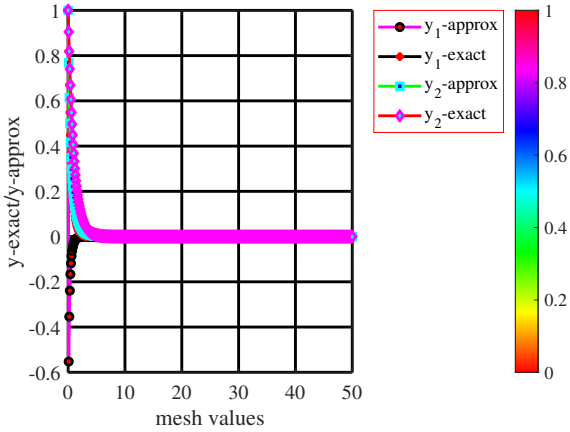

Figure 82: The accuracy curves of Problem 6.5 when $x \in [0,50]$ for COT4

7. Conclusion and future research

In this research, single intra-step optimal block methods are proposed with a uniform algebraic convegence order of 4. The numerical experiments clearly show that the proposed COT methods consistently outperform existing approaches across a range of test problems, such as biomass transfer in trees and nutrient flow in aquariums. The results highlight significant accuracy gains, with rapidly decreasing errors as step sizes are refined, while solution plots and precision factors confirm stability and reliability. Among the schemes, COT4 stands out, achieving the lowest error levels and highest precision factor values, making it the most efficient and accurate of the class. When compared with the NPOBM scheme, the COT methods, especially COT4, demonstrate superior accuracy, stability, and efficiency without added computational cost. Their strong performance in both linear and nonlinear systems, including stiff dynamics, underscores their robustness and suitability for real-life applications. These findings validate the proposed methods as effective alternatives for solving complex differential systems, while future work may extend them to larger coupled systems, fractional-order models, and adaptive step-size frameworks for enhanced efficiency.

Funding

The authors did not receive any specific support from any funding agencies in the public, commercial, or not-for-profit sectors for the submitted work.

Conflict of interests

The authors declare that there are no financial or non-financial interests that are relevant to the content of this article.

Availability of data

The data used to support the results of the study are sourced from literature and enclosed in the references section.

Acknowledgement

The authors sincerely thank the anonymous reviewers for their insightful comments and constructive suggestions, which have strengthened this work.

Author contributions

O. V. Atabo, Conceptualization, methodology, former analysis and software. A. T. Cole, validity and visualization. S. O. Adee, validity and confirmation. P. O. Olatunji, investigation,

review and editing. E. O. Omole, visualization and confirmation. Q. O. Ahman, original draft preparation. All content of manuscript were written via author's contribution, read and agreed to publish the final manuscript.

References

[1] Henrici, P. (1962). *Discrete variable methods in ordinary differential equations*. New York, NY: John Wiley & Sons.

[2] Lyu, W., & Wang, Z. A. (2022). Logistic damping effect in chemotaxis models with density-suppressed motility. *Advances in Nonlinear Analysis, 12*, 336–355. https://doi.org/10.1515/anona-2022-0263

[3] Hussain, K., Amourah, A., Salah, J., Jameel, A. F., & Anakira, N. (2025). Autonomous block method for uncertainty analysis in first-order real-world models using fuzzy initial value problems. *AIMS Mathematics, 10*(4), 9614–9636. https://doi.org/10.3934/math.2025443

[4] Gbenro, S. O., Areo, E. A., & Momoh, A. L. (2025). An accurate two-step optimized hybrid block method for integrating stiff differential equations. *American Journal of Applied Mathematics, 13*(1), 64–72. https://doi.org/10.11648/j.ajam.20251301.15

[5] Singla, R., & Singh, G. (2024). An efficient optimized adaptive step-size hybrid block method for integrating $w'' = f(t, w, w')$. *Journal of Computational and Applied Mathematics, 420*, 1–19. https://doi.org/10.1016/j.cam.2022.114838

[6] Motsa, S., Ahmedai, S., Nefale, M., & Otegbeye, O. (2024). A rational optimal block hybrid method for enhanced accuracy in solving Lane-Emden equations. *Partial Differential Equations in Applied Mathematics, 12*, 101003. https://doi.org/10.1016/j.padiff.2023.101003

[7] Emmanuel, S. (2024). Leveraging feed-forward neural networks to enhance the performance of hybrid block methods for first-order initial value problems. *Applied Mathematics and Computation, 423*, 1–15. https://doi.org/10.1016/j.amc.2022.127134

[8] Adoghe, L. O., Ukpebor, L., Ononogbo, B., & Airemen, E. (2024). A one-step hybrid Obrechkoff-type block method for first-order initial value problems in ordinary differential equations. *HyperSoft Set Methods in Engineering, 1*, 84–94. https://doi.org/10.61356/j.hsse.2024.111850

[9] Rufai, M. A. (2023). A new hybrid block method for solving first-order initial value problems. *Mathematics, 11*(7), 703. https://doi.org/10.3390/math11070703

[10] Duromola, M. K., Lawal, R. S., & Akinmoladun, O. M. (2024). Numerical integration of linear hybrid multistep block method for third-order ordinary differential equations (IVPs). *Scientific African, 24*, e02129. https://doi.org/10.1016/j.sciaf.2024.e02129

[11] Duromola, M. K., Momoh, A. L., & Kusoro, O. O. (2024). A modified fourth derivative block method and its direct applications to third-order initial value problems. *Journal of Mathematical Analysis and Modeling, 4*(3), 63–75. https://doi.org/10.48185/jmam.v4i3.897

[12] Odeyemi, J. K., Olaiya, O. O., & Ogunfiditimi, F. O. (2023). Hermite polynomial-based methods for optimal order approximation of first-order ordinary differential equations. *Journal of Advances in Mathematics and Computer Science, 38*(6), 16–32. https://doi.org/10.9734/JAMCS/2023/v38i61765

[13] Kayode, S. J., Obarhua, F. O., & Odaodu, F. T. (2025). A three-step hybrid block method for direct integration of third-order ordinary differential equations. *Scholars Journal of Physics and Mathematics, 12*(1), 11–23. https://doi.org/10.36347/sjpms.2025.v12i01.003

[14] Orapine, H. O., Donald, J. Z., Baidu, A. A., & Oladele, J. O. (2024). A new hybrid block method via combined Hermite polynomials and exponential functions as basis function. *Ikonion Journal of Mathematics, 2*(5), 10–23. https://doi.org/10.54286/ikjm.1227629

[15] Kwari, L. J., Sunday, J., Ndam, J. N., Shokri, A., & Wang, Y. (2023). On the simulations of second-order oscillatory problems with applications to physical systems. *Axioms, 12*(3), 282. https://doi.org/10.3390/axioms12030282

[16] Raymond, D., Pantuvu, T. P., Lydia, A., Sabo, J., & Ajia, R. (2023). An optimized half-step scheme third derivative methods for testing higher order initial value problems. *African Scientific Reports, 2*(76), 1–8. https://doi.org/10.46481/asr.2023.2.1.76

[17] Yakubu, S. D., & Sibanda, P. (2024). One-step family of three optimized second-derivative hybrid

block methods for solving first-order stiff problems. *Journal of Applied Mathematics, 2024*, 5078943. https://doi.org/10.1155/2024/5078943

[18] Ayinde, A. M., Ibrahim, S., Sabo, J., & Silas, D. (2023). The physical application of motion using single step block method. *Journal of Material Science Research and Review, 6*(4), 708–719. https://journaljmsrr.com/index.php/JMSRR

[19] Donald, J. Z., Skwame, Y., Sabo, J., & Ayinde, A. M. (2021). The use of linear multistep method on implicit one-step second derivative block method for direct solution of higher order initial value problems. *Abacus (Mathematics Science Series, 48)*(2), 224–237.

[20] Igbinovia, E., Ogunfeyitimi, S. E., & Ikhile, M. N. O. (2025). Block hybrid trapezoidal-type methods for solving initial value problems. *Earthline Journal of Mathematical Sciences, 15*(3), 345–365. https://doi.org/10.34198/ejms.15325.345365

[21] Sabo, J., Kyagya, T. Y., & Vashawa, W. J. (2021). Numerical simulation of one step block method for treatment of second-order forced motions in mass spring systems. *Asian Journal of Research and Reviews in Physics, 5*(2), 1–11. https://doi.org/10.9734/ajr2p.2021/v5i230157

[22] Olabode, B. T., Kayode, S. J., Olatubi, O. J., & Momoh, A. L. (2024). Advancing numerical methods of block multi-derivative approaches for ODEs of various orders. *Asian Research Journal of Mathematics, 20*(6), 1–14. https://doi.org/10.9734/arjom/2024/v20i6803

[23] Akinola, R. O., Omole, E. O., Sunday, J., & Kutchina, S. Y. (2025). A ninth-order first derivative method for numerical integration. *Journal of the Nigerian Society of Physical Sciences, 7*, 2028. https://doi.org/10.46481/jnsps.2025.2028

[24] Abuasbeh, K., Qureshi, S., Soomro, A., & Awadalla, M. (2023). An optimal family of block techniques to solve models of infectious diseases: Fixed and adaptive stepsize strategies. *Mathematics, 11*, 1135. https://doi.org/10.3390/math11051135

[25] Akinnukawe, B. I., & S. A. (2024). One-step block scheme with optimal hybrid points for numerical integration of second-order ordinary differential equations. *Journal of the Nigerian Society of Physical Sciences, 6*, 1827. https://doi.org/10.46481/jnsps.2024.1827

[26] Lambert, J. D. (1991). *Numerical methods for ordinary differential systems: The initial value problem*. Hoboken, NJ: John Wiley & Sons, Inc.

[27] Abramowitz, M., & Stegun, I. A. (1964). *Handbook of mathematical functions with formulas, graphs, and mathematical tables* (10th printing). Washington, DC: U.S. National Bureau of Standards, Applied Mathematics Series, 1–1046.